

**STUDY OF AUTOMOTIVE RADIATOR COOLING SYSTEM FOR A
DENSE-ARRAY CONCENTRATION PHOTOVOLTAIC SYSTEM**

By

TAN WOEI CHONG

A thesis submitted to the
Department of Electrical and Electronic Engineering,
Faculty of Engineering and Science,
Universiti Tunku Abdul Rahman,
in partial fulfillment of the requirements for the degree of
Master of Engineering Science
April 2013

ABSTRACT

STUDY OF AUTOMOTIVE RADIATOR COOLING SYSTEM FOR A DENSE-ARRAY CONCENTRATION PHOTOVOLTAIC SYSTEM

Tan Woei Chong

A cost effective and off-the-shelf active cooling device for dense-array Concentrator Photovoltaic (CPV) system was introduced and developed. Automotive radiator was chosen as the main heat rejection device of the active cooling system due to the high heat dissipation profile. Besides that, its parasitic load is low compared to other cooling devices such as industrial cooling tower and chiller. The automotive radiator is also easily available, light weight and compact, hence easy to develop. The cooling fluid of the system is water which is easily obtained and non-toxic. To obtain the optimize specifications and feasibility of the automotive cooling system, theoretical analysis and on-site experimental data collection have been conducted. Theoretical study of the automotive radiator was carried out to analyze the automotive radiator's heat rejection rate in the function of temperature difference between radiator and ambient for different water flow rates and wind speeds created by fan. Besides that, the performance of the designed cooling block was studied using CFD program and analytical formulas.

To verify the theoretical modeling of the automotive radiator cooling system, on-site data collections were conducted using prototype NIPC with total reflective area of 4.16 m^2 and solar concentration ratio of 377 suns. Other than that, an experiment was conducted to obtain the relationship between the electrical conversion efficiency of CPV module and the cell temperature. From the experiment, the electrical conversion efficiency of CPV module is inversely proportional to the CPV cell temperature in which the conversion efficiency reduces about 0.14% for every $1 \text{ }^\circ\text{C}$ increment in the temperature. For the prototype NIPC, the highest net electrical power output was 665.3 W provided that solar power input was 3118.7 W and conversion efficiency was 26.16 %.

ACKNOWLEDGEMENT

First and foremost, I would like to take this opportunity to express my sincere appreciation and deepest gratitude to my supervisor, Dr. Chong Kok Keong, for his guidance, invaluable advice, understanding and considerations on my works. I was able to gain a lot of experiences, skills and knowledge from him.

I wish to express my gratitude to Prof. Dr Faidz bin Abd Rahman, my co-supervisor. He had provided me continuous guidance, directions and advice when I was conducting my works. I would also wish to indicate special gratitude and deepest thankfulness to my research's partners, Wong Chee Woon, Tan Ming Hui, Jessie Siaw Fei Lu, Yew Tiong Keat and Chong Yee How, for their assistances. They always give me support, encouragement and advice according to their technical expertise and experience.

To my beloved family, appreciate for the encouragement and mentally support throughout the duration of my study. Last but not the least, with sincere affection and love to my friends, thank you for your friendship, constant encouragement and invaluable help, I wish you all great blessing.

APPROVAL SHEET

This thesis entitled "**STUDY OF AUTOMOTIVE RADIATOR COOLING SYSTEM FOR A DENSE-ARRAY CONCETRATION PHOTOVOLTAIC SYSTEM**" was prepared by TAN WOEI CHONG and submitted as partial fulfillment of the requirements for the degree of Master of Engineering and Science at Universiti Tunku Abdul Rahman.

Approved by:

(Prof. Dr. CHONG KOK KEONG)

Date:.....

Supervisor

Department of Electrical and Electronic Engineering

Faculty of Engineering and Science

Universiti Tunku Abdul Rahman

(Prof. Dr. FAIDZ BIN ABD RAHMAN)

Date:.....

Co-supervisor

Department of Electrical and Electronic Engineering

Faculty of Engineering and Science

Universiti Tunku Abdul Rahman

FACULTY OF ENGINEERING AND SCIENCE
UNIVERSITI TUNKU ABDUL RAHMAN

Date: 1 April 2013

SUBMISSION OF THESIS

It is hereby certified that **TAN WOEI CHONG** (ID No: **10UEM07353**) has completed this thesis entitled " STUDY OF AUTOMOTIVE RADIATOR COOLING SYSTEM FOR A DENSE-ARRAY CONCENTRATION PHOTOVOLTAIC SYSTEM" under supervision of Prof. Dr. Chong Kok Keong (Supervisor) from the Department of Electrical and Electronic Engineering, Faculty of Engineering and Science, and Prof. Dr. Faiz Bin Abd Rahman (Co-Supervisor) from the Department of Electrical and Electronic Engineering, Faculty of Engineering and Science.

I understand that University will upload softcopy of my thesis in pdf format into UTAR Institutional Repository, which may be made accessible to UTAR community and public.

Yours truly.

(TAN WOEI CHONG)

DECLARATION

I hereby declare that the dissertation is based on my original work except for quotations and citations which have been duly acknowledged. I also declare that it has not been previously or concurrently submitted for any other degree at UTAR or other institutions.

Name : Tan Woei Chong

Date : 1 October 2012

TABLE OF CONTENTS

	Page
ABSTRACT	ii
ACKNOWLEDGEMENT	iv
APPROVAL SHEET	v
SUBMISSION OF THESIS	vi
DECLARATION	vii
TABLE OF CONTENTS	viii
LIST OF TABLES	xii
LIST OF FIGURES	xiii
LIST OF ABBREVIATIONS	xvii
 CHAPTER	
1.0 INTRODUCTION	1
1.1 Research Background	1
1.2 Research Objective	7
1.3 Thesis Overview	8

2.0	LITERATURE REVIEW	9
2.1	CPV Module Configurations	9
2.1.1	Single Cell	9
2.1.2	Linear Geometry	11
2.1.3	Dense-array	12
2.2	Non-imaging Planar Concentrator (NIPC)	14
2.2.1	Principle and NIPC	14
2.2.2	Method of Sun Tracking	16
2.3	Automotive Radiator	17
2.4	Cooling Tower	19
2.5	Heat Transfer	19
2.5.1	Conduction	20
2.5.2	Radiation	21
2.5.3	Convection	22
	2.5.3.1 Heat Transfer Coefficient	24
	2.5.3.2 Nusselt Number	25
	2.5.3.3 Reynolds Number	26
2.6	Computational Fluid Dynamics (CFD)	27
2.6.1	Standard K – epsilon Turbulent Model	27
3.0	METHODOLOGY	29
3.1	Theoretical Study	29

3.1.1	Theoretical Study of Heat Transfer of Automotive Radiator	30
3.1.2	Theoretical Study of Heat Transfer of Cooling Block	33
3.2	Computational Fluid Dynamic Simulation of 3-D Modeling Cooling Block	35
3.3	Experimental Setup	37
3.3.1	Construction of NIPC	38
3.3.1.1	Specification of NIPC	38
3.3.1.2	Tracking Method of NIPC	41
3.3.1.3	Flux Distribution of NIPC	43
3.3.2	Automotive Radiator Cooling System	46
3.4	Data Collection and Experiments	53
4.0	RESULT and DISCUSSIONS	58
4.1	Results of Theoretical Study	58
4.1.1	Result of Theoretical Study of Automotive Radiator	58
4.1.2	Result of Theoretical Study of Cooling Block	60
4.2	Result of Data Collection and Experiment	63
4.2.1	Real-time Data Collection	63
4.2.2	Comparison between Theoretical Result and	67

	Experimental Result	
4.2.3	CPV Module Conversion Efficiency	68
4.3	Comparison of Automotive Radiator Cooling System to Cooling Tower	70
5.0	CONCLUSION	75
5.1	Concluding Remarks	75
5.2	Future Work	77
	REFERENCES	78
	APPENDICES	
A	Study of Automotive Radiator Cooling System for Dense-array Concentration Photovoltaic System	86
B	Sewage Submersible Pump	98
C	QB 60 Booster Pump 220V 370W	100

LIST OF TABLES

Table		Page
3.1	The specification of experimental setup (Chong and Tan, 2012).	52
4.1	Comparison between automotive radiator cooling system and small size cooling tower.	71

LIST OF FIGURES

Figure		Page
2.1	The schematic diagram of a single CPV cell system illuminated under high concentration sunlight with focusing lens as entrance aperture (Royne <i>et al.</i> , 2005).	10
2.2	The schematic diagram of a linear geometry CPV cell system illuminated under high concentration sunlight with linear focusing lens as entrance aperture (Royne <i>et al.</i> , 2005).	12
2.3	Schematic diagram of dense-array CPV module illuminated under high concentration sunlight with entrance aperture (Royne <i>et al.</i> , 2005).	13
2.4	Conceptual layout of NIPC and Cross-sectional view of NIPC to show how the individual mirror directs the sunlight to the receiver, (a) isometric view, (b) side view (Chong <i>et al.</i> , 2009a).	15
2.5	Schematic diagram of the setup of AE tracking method NIPC (Chong <i>et al.</i> , 2009a).	17
2.6	Schematic diagram of automotive radiator.	18

3.1	Drawing to show the numerical modeling of the cooling block where its domains comprises of three major parts of the cooling block with slot fins, cooling block cover and water acting as cooling fluid (Chong and Tan, 2012).	35
3.2	Picture to show the prototype of nonimaging planar concentrator that is located along the south-north orientation at latitude of 3.2° N and longitude of 107.7° E, in the campus of Universiti Tunku Abdul Rahman (UTAR), Kuala Lumpur, Malaysia (Chong and Tan, 2012).	39
3.3	Windows-based program implemented using Microsoft Visual Basic.net developed to control the sun-tracking mechanism according to the day number of the year, the local time, time zone, latitude and longitude of the prototype installation (Chong and Tan, 2012).	42
3.4	The concentrated sunlight has generated different grades of burnt mark on the sand paper, where the total area of burnt mark on the sand paper was measured as 11 cm × 11 cm and a darker carbonized burnt area was measured as 8.8 cm × 8.8 cm (Chong and Tan, 2012).	44
3.5	The simulation results of solar flux distribution for the prototype nonimaging planar concentrator that consisted of 420 flat mirrors in (a) 3-D and (b) 2-D plots with a focal distance of 170 cm (Chong and Tan, 2012).	45

3.6	Picture to show the automotive radiator from a commercial automobile “Proton Wira 1500 c.c.” with the capacity of 1500 c.c to be used as the key device for the heat rejection in the cooling system (Chong and Tan, 2012).	47
3.7	Drawing to show the cooling block made of a copper with a dimension 180 mm × 146 mm × 20 mm to be machined into a pattern of multiple water channels (Chong and Tan, 2012).	49
3.8	The schematic diagram to show all the components of the automotive radiator cooling system and the flow direction of water in the experimental setup (Chong and Tan, 2012).	51
3.9	The left photo shows how the CPV module is attached on cooling block for on-site measurement and the right photo shows the CPV module exposed under high solar concentration during on-site measurement (Chong and Tan, 2012).	55
4.1	The graphs of heat rejection rate of automotive radiator versus temperature difference between radiator and ambient for different wind speeds and the heat transfer area of radiator (Chong and Tan, 2012).	59
4.2	The graphs of temperature at the center of cooling block versus solar heat flux input for different water inlet temperature and mass flow rate. (Solid line represents mass flow rate of 0.4 kgs ⁻¹ and dot line represents mass flow rate of 0.583 kgs ⁻¹) (Chong and Tan, 2012).	61

4.3	The graphs of solar power input, heat rejection rate and the temperature at the center of cooling block versus time (minutes) in the first experiment (Chong and Tan, 2012).	64
4.4	The graphs of solar power input, heat rejection rate and the temperature at the center of cooling block versus lock clock time for a period of 6 hours at the interval of 15 minutes in the second experiment (Chong and Tan, 2012).	65
4.5	The graphs to show a comparison for the heat rejection rate of radiator between experimental and theoretical results (Chong and Tan, 2012).	67
4.6	Graph to show the measurement result of electrical conversion efficiency of CPV module versus CPV cell temperature (Chong and Tan, 2012).	69

LIST OF ABBREVIATIONS

A	Total surface area of heat transfer, m ² .
A_c	Cross-sectional area, m ² .
A_r	Total area of mirrors which reflect the solar flux to the target of NIPC, m ² .
c	Heat capacity of water, J kg ⁻¹ K ⁻¹ .
D_h	Hydraulic diameter, m.
DNI	Direct normal irradiance, Wm ⁻² .
h	Heat transfer coefficient, Wm ⁻² K ⁻¹ .
I_{sc}	Short circuit current, A.
k	Turbulent kinetic energy, m ² s ⁻² .
k_a	Thermal conductivity of air, Wm ⁻¹ K ⁻¹ .
$k_{\text{DBC-alumina}}$	Thermal conductivity of alumina layer in direct bond copper (DBC) substrate, Wm ⁻¹ K ⁻¹ .
$k_{\text{arctic silver}}$	Thermal conductivity of arctic silver thermal adhesive, Wm ⁻¹ K ⁻¹ .
k_{CPV}	Thermal conductivity of CPV cell, Wm ⁻¹ K ⁻¹ .
k_{copper}	Thermal conductivity of copper cooling block, Wm ⁻¹ K ⁻¹ .
k_{solder}	Thermal conductivity of solder, Wm ⁻¹ K ⁻¹ .
$k_{\text{DBC-copper}}$	Thermal conductivity of copper layer in direct bond copper (DBC) substrate, Wm ⁻¹ K ⁻¹ .

k_w	Thermal conductivity of water, $\text{Wm}^{-1}\text{K}^{-1}$.
L	Length parallel to the water flow direction in cooling block.
\dot{m}	Mass flow rate of water, kgs^{-1} .
Nu_a	Nusselt number of forced convection within radiator and air.
Nu_w	Nusselt number of forced convection within cooling block and water.
P	Perimeter, m.
p	Pressure, Nm^{-2} .
P_{in}	Solar power input, W.
$P_{\text{CPV,in}}$	Solar power input to single cell module, W.
$P_{\text{CPV,out}}$	Electricity power output by single cell module, W.
Pr_a	Prandtl number (based on air temperature).
Pr_w	Prandtl number (based on water temperature).
Pr_s	Prandtl number (based on radiator surface temperature).
$Q_{\text{convection}}$	Convection heat transfer, W.
ΔT	Temperature difference, $^{\circ}\text{C}$.
ε_t	Turbulent energy dissipation rate, m^2s^{-2} .
ε	Surface emissivity.
μ_a	Dynamic viscosity of air, Nsm^{-2} .
μ_w	Dynamic viscosity of water, Nsm^{-2} .
η	The efficiency of direct conversion from solar energy to thermal energy.
ρ	Fluid density, kgm^{-3} .

ρ_a	Air density, kgm^{-3} .
ρ_w	Water density, kgm^{-3} .
σ	Stefan-Boltzmann constant, $\text{Wm}^{-2}\text{K}^{-4}$.
σ_k, σ_s	Turbulent constant.
σ_l	Laminar Prandtl number.
σ_t	Turbulent Prandtl number.

CHAPTER 1

INTRODUCTION

1.1 Research Background

High Concentrator Photovoltaic (HCP) is one of the most effective devices to reduce the cost in solar power generation. In these systems, the HCP solar cells exposed to high solar illumination can claim higher conversion efficiency (Zahedi, 2010) (Chong and Tan, 2012). This can reduce the expensive solar cell area by replacing with a cost effective concentrator material. Under high concentrated sunlight, the solar cells will inevitably experience a very high heat load that can decrease the conversion efficiency if the solar cells' temperature is not properly managed (Dalal and Moore, 1977; Mbewe *et al.*, 1985; Sala, 1989) (Chong and Tan, 2012). According to Cui *et al.* (2009), a single solar cell can reach extremely high temperatures up to 1200°C with the absence of cooling system at 400 suns, whilst the temperature can be reduced dramatically by attaching it to a metal panel as cooling panel. Therefore, a reliable heat dissipation system is necessary in HCPV system to continuously cool the solar cells effectively in order to maintain their best performance in all times (Royne *et al.*, 2005) (Chong and Tan, 2012). To achieve the goal, many different cooling techniques have been developed. Different cooling

techniques might have different performance and not all of the cooling techniques are applicable for HCP system including dense-array CPV system. For dense-array CPV system, a very rapid cooling is required (Chong and Tan, 2012).

In the current HCP system, there are two types of heat dissipation system widely utilized namely passive and active cooling systems (Liu *et al.*, 2011) (Chong and Tan, 2012). Passive cooling is the cooling method for photovoltaic cell by applying radiation or natural convection (discussed in Section 2.4.2 and 2.4.3) to transfer the excess heat from photovoltaic cell to maintain it in low temperature in order to maintain the cell conversion efficiency, therefore it has no other external forces such as pumping force acting along the cooling. Since, radiation or natural convection are applied, therefore the heat transfer rate would not be higher than the active cooling and only applicable for single cells geometry or linear geometry (discussed in Section 2.1.1 and 2.1.2).

Active cooling is the cooling method in which forced convection is applied to dissipate the extra heat from photovoltaic cells. Since forced convection is applied, there are external forces acting on the cooling system such as pump is used to pump the cooling fluid pass through the heat sink of cell to absorb the excess heat from the cell. With the assistance of external forces, the heat transfer rate of active cooling will be high and this cooling method is able to be applied in dense-array geometry (discussed in section 2.1.3).

In the categories of passive cooling system, Araki *et al.* (2002) developed a passive heat dissipation device which can dissipate solar cells' heat operating under 500 suns. An American patented cooling system by Fork *et al.* (2007) is able to cool the solar cells passively under multi-reflective concentrations with large thermal radiation surface area. Aas and Hansen (2008) patented a cooling apparatus for photovoltaic panels. The basis layer of the US Patent cooling apparatus was designed with many protruding structure which fixed to back side of panels (Chong and Tan, 2012).

Other than that, Edenburn (1980) performed a cost-efficiency analysis of small point-focus Fresnel lens array geometry with passive cooling system. The design of the cooling device is linear fins erected on all the heat sink's available top surface (Chong and Tan, 2012). The solar concentration ratios in the analysis are 50, 92 and 170 suns. Minano *et al.* (1994) presented a passive cooling device for a single cell under high solar concentrations. As similar to Edenburn (1980), he made a conclusion that the efficiency of cooling device increases when the size of solar cells is reduced. Moreover, Minano *et al.* (1994) advised that the cells' diameter should be kept below 5 mm and the cooling device would be similar to those used for power semiconductor devices. For passive cooling in linear array solar cell geometry, Luque *et al.* (1997) propose a trough-type photovoltaic concentrator technology-EUCLIDES. In this particular system, the thermal energy is passively dissipated to the ambient through a lightweight aluminum-finned heat sink that

have been optimized for low concentration (about 30 suns). Most of the passive cooling systems are applied in single solar cell geometry or linear array solar cell geometry, but there was no report on the passive cooling system applied under dense array solar cells geometry with very high solar illumination (Royne *et al.*, 2005) (Chong and Tan, 2012).

Dense array solar cells always encounter high thermal energy and consequently most of the passive cooling systems lost their function for dense array geometry. Active cooling systems are applicable in this particular geometry. Lasich (2002) patented an active cooling system with water circulation for densely array solar cells under high solar concentration. The water circuit is claimed to be able to dissipate 500 kWm^{-2} from the solar cells and maintain the temperature of solar cell around 40°C under normal operating conditions. The concept is based on water flow through small and parallel channels in thermal contact with solar cells (Chong and Tan, 2012).

From 2002 to 2003 Vincenzi *et al.* at the University of Ferrara have proposed micro-machined silicon heat sinks for their concentrator system (Vincenzi *et al.*, 2002, 2003). The dense-array solar cells panel with the dimension of $30 \times 30 \text{ cm}^2$ operates at 120 suns concentration, by using a silicon wafer with micro-machined channels, the water is circulated directly underneath the solar cells and the thermal resistance of the heat sink reported is $4 \times 10^{-5} \text{ Km}^2\text{W}^{-1}$. Horne

(1993) patented a system with a paraboloidal dish to focus the sunlight onto the solar cells. Instead of being mounted on a horizontal surface, they are mounted vertically on a set of rings that are designed to cover the receiving area without shadowing. Water is transported up to the receiver by central pipe and then flows behind the solar cells before return. In this way, the water can cool the solar cells and absorbing UV radiation concurrently (Chong and Tan, 2012).

Royne and Dey (2007) proposed a cooling device for dense array photovoltaic cells under high solar concentration based on the concept of jet impingement. The cooling device consists of an array of jets where the cooling fluid is drained around the sides in the direction normal to the jet impinged surface. An experiment was set-up to measure the local and average heat transfer coefficient as well as pressure drop of the device. Extensive literature reviews of jet impingement were given and among others are Martin (1977), Webb and Ma (1995), Jambunathan *et al.* (1992), Royne *et al.* (2005). Other than that, Ryu *et al.* (2002) has presented a cooling method by applying the concept of microchannel heat sinks with dimension of $1 \times 1 \text{ cm}^2$ with the lowest reported thermal resistance is $9 \times 10^{-6} \text{ Km}^2\text{W}^{-1}$. The associated pressure drop is 103.42 kPa and the optimal dimensions are 320 μm channel depth, 56 μm channel width and 44 μm wall width. Apply microchannel cooling device in dense-array CPV is very costly. It is because most of the dimensions in microchannel device are less than 1 mm, the fabrication of the microchannel will be tedious and costly. By the way, microchannel's thermal

resistance is low, therefore the temperature of CPV can be reduced dramatically.

According to Barrau *et al.* (2011), the cooling device is combined with a slot jet impingement and non-uniform distribution of micro-channel. The minimum value of thermal resistance coefficient obtained is $2.18 \times 10^{-5} \text{ Km}^2\text{W}^{-1}$ for the cooling device. The net PV output with the area of PV 576 cm^2 for 610 suns and 1905 suns are 7905.6 W and 23817.6 W respectively (Chong and Tan, 2012).

On the other hand, Zhu *et al.* (2009) proposed an efficient liquid-immersion cooling method for heat dissipation of dense array solar cells at high solar concentration level. The direct-contact heat transfer performance was investigated under different solar concentration level, liquid temperatures and fluid flow velocities. Since the solar cells are immersed in the water, the water used must be a dielectric water to avoid short circuit and oxidation of solar cells. In such a way, the cost will increase due to dielectric water is more difficult to prepare. Moreover, the fabrication of CPV module will become complicated due to immersion in water. The cost of fabrication will increase also.

Here, we would like to explore a cost effective and off-the-shelf active cooling system for dense-array Concentrator Photovoltaic (CPV) system, which is an automotive radiator to be built into the cooling system as the main component of heat rejection of solar cells. Automotive radiator has high heat dissipation profile

and does not consume high power like other cooling devices such as industrial cooling tower and chiller. The automotive radiator has lower cost, easily available, light weight and compact, and hence the proposed setup of cooling system is easy to establish. In addition, water can be used as service fluid, which is non-toxic, easily obtained and not as complex as dielectric water proposed by Zhu *et al.* (2010). Therefore, for the prototype NIPC, automotive radiator is a cost effective cooling device (Chong and Tan, 2012).

1.2 Research Objective

The objectives of the study:

1. To construct a non-imaging planar concentrator (NIPC) to serve the purpose of sun tracking and sunlight reflecting.
2. To integrate an automotive radiator as part of the cooling system for a dense-array CPV system and installation of the proposed cooling system on the NIPC.
3. To accomplish theoretical analysis and on-site data collection of the automotive radiator cooling system to confirm the optimized specifications and verify the feasibility of the automotive radiator cooling system.

4. To measure the conversion efficiency of concentrator photovoltaic module under different operating temperature to justify the significance of cooling system in maintaining the good performance of CPV system.

1.3 Thesis Overview

The organization of the thesis is as follow: Chapter 1 of this thesis gives an introduction and general idea of the research and clarifies the research objectives. Chapter 2 gives the literature review about the concentration photovoltaic (CPV) cell arrays, non-imaging planar concentrator (NIPC) and automotive radiator. In addition, the formula used to calculate the heat transfer and computational fluid dynamic (CFD) also reviewed. In Chapter 3, the methodology for theoretical study and data collection were discussed in detail. The application of formula in theoretical study and data collection were discussed. The setup for NIPC and cooling system also is included in this chapter. The results of theoretical study and data collection were shown and discussed in Chapter 4. Besides that, it also included the comparison between automotive radiator and cooling tower. Chapter 5 is ending the thesis with conclusions and included future works.

CHAPTER 2

LITERATURE REVIEW

2.1 CPV Module Configurations

The CPV module can be categorized into three configurations which are single cell configuration, linear geometry and dense-array. They are categorized according to method of concentrating (mirrors or lenses), level of sunlight concentration and array of CPV cells geometry (Royne *et al.*, 2005).

2.1.1 Single Cell

In small point-focus concentrators, sunlight is always focused onto one CPV cell individually (Royne *et al.*, 2005). This means that the area of focused sunlight onto each CPV cell must be almost equal or slightly bigger than the area of CPV cell to make sure each of the CPV cell is fully illuminated under high concentration sunlight. Commonly, single cell systems apply various types of lenses to concentrate sunlight onto single CPV cell and Fresnel lens is the most used one. Another option is where the reflective concentrators transmit the

concentrated light through optical fibers onto single CPV cells. For single CPV cell system, passive cooling is recommended for the concentration less than 150X. Edenburn (1980) had introduced active cooling for single CPV cell system. Figure 2.1 is the schematic diagram which shows a single CPV cell is illuminated under high concentration sunlight with focusing lens as entrance aperture.

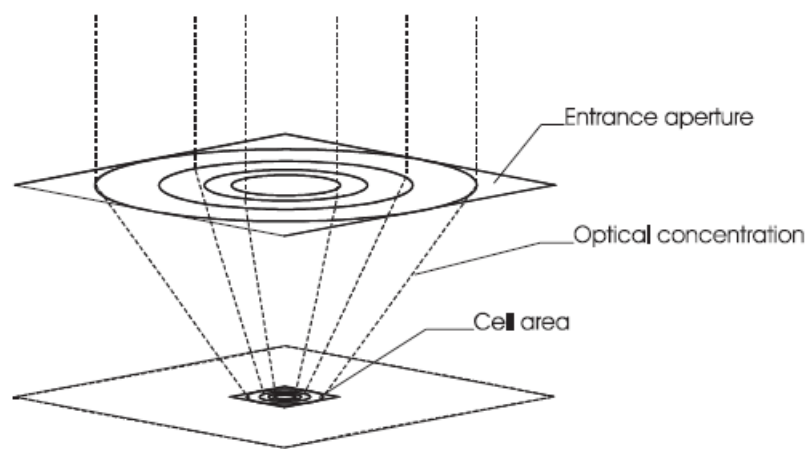


Figure 2.1: The schematic diagram of a single CPV cell system illuminated under high concentration sunlight with focusing lens as entrance aperture (Royne *et al.*, 2005).

2.1.2 Linear Geometry

Linear geometry refers to CPV cells which are arrayed in a row of straight line and each of the CPV cells is very close to their neighbouring cells. In linear geometry, parabolic troughs or linear Fresnel lenses are the most typical method used to focus the sunlight onto a row of CPV cells. With this linear geometry, the CPV cells have less area available for heat dissipating due to two of the CPV cell sides which are very close contact with the neighbouring cells. The only areas available for heat dissipation are extending from two of the sides or the back side of the CPV cells (Royne *et al.*, 2005). The cooling methods for linear geometry can be either passive cooling or active cooling. Edenburn (1980) suggested both active and passive cooling system for this linear geometry design (Royne *et al.*, 2005). Figure 2.2 is the schematic diagram shows a row of CPV cells arrayed in a straight line and illuminated under high concentration sunlight with linear focusing lens as entrance aperture.

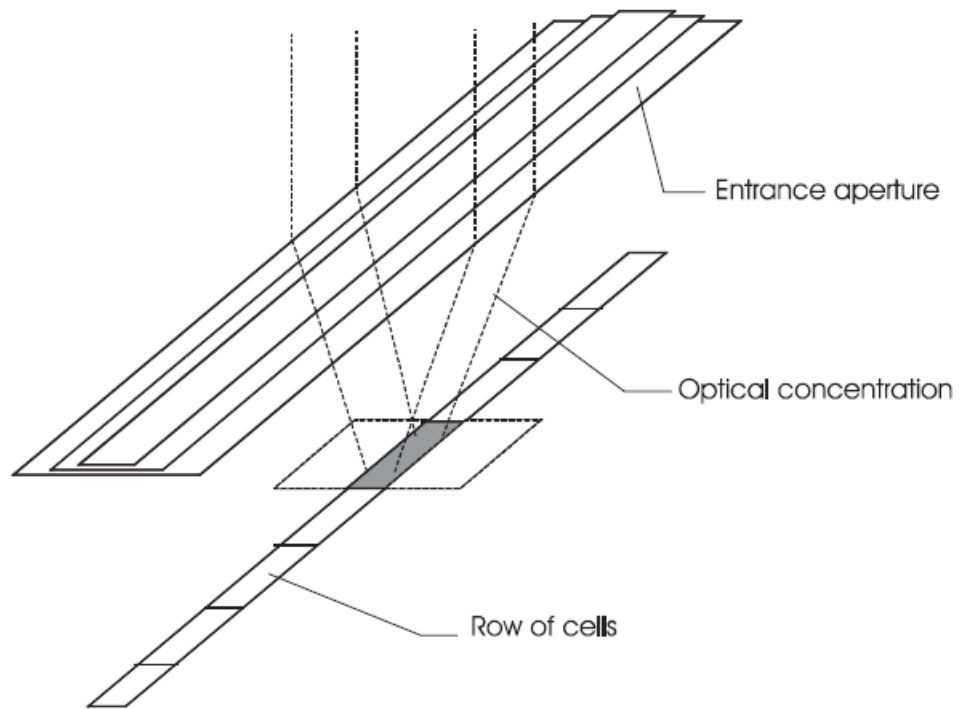


Figure 2.2: The schematic diagram of a linear geometry CPV cell system illuminated under high concentration sunlight with linear focusing lens as entrance aperture (Royne *et al.*, 2005).

2.1.3 Dense-array

In larger point-focus systems, such as parabolic dishes, heliostat fields or non-imaging planar concentrator (NIPC) discussed in Section 2.2, generally, the receiver consists of a multitude of densely packed CPV cells which the CPV cell are very close contact with the neighbouring cells in every sides with a fine gap. The receiver is usually placed slightly away from the focal plane to obtain a

uniform illumination (Chong *et al.*, 2010). By option, secondary concentrators (kaleidoscopes) may be used to further improve flux homogeneity (Kreske, 2002). Dense-array CPV modules present greater problems for cooling than the two previous configurations discussed. Except the edge of CPV cells, each of the CPV cells only has its back side available for heat dissipation (Royne *et al.*, 2005). Moreover, the area of illumination onto the dense-array CPV modules and level of sunlight concentration are always larger than the previous configuration. Therefore the excess energy converted to heat would be the highest. Only an effective active cooling is suitable to apply for dense-array CPV module (Royne *et al.*, 2005). Figure 2.3 is the schematic diagram of dense-array CPV module illuminated under high concentration sunlight with entrance aperture.

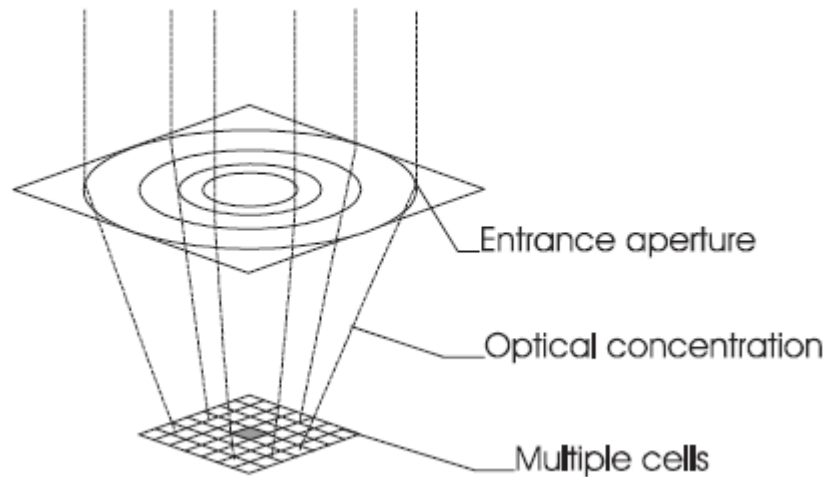


Figure 2.3: Schematic diagram of dense-array CPV module illuminated under high concentration sunlight with entrance aperture (Royne *et al.*, 2005).

2.2 Non-imaging Planar Concentrator (NIPC)

Concentrator plays an important role for focusing sunlight onto receiver for any solar power generation station. Non-imaging planar concentrator (NIPC) is one of the concentrator able to achieve the objective. To concentrate sunlight onto dense-array CPV module as discussed in Section 2.1.3, is required. The design and construction of NIPC is further discussed in Section 3.3.1.

2.2.1 Principle and Concept of NIPC

To achieve a high concentration solar irradiation with good uniformity onto the dense-array CPV module, NIPC was proposed. This NIPC is formed by numerous flat mirrors acting as entrance aperture to collect and focus the incident sunlight onto the receiver which is installed above the focal plane (Chong *et al.*, 2009a). The focal length is adjusted to obtain optimum sunlight concentration and uniform illumination (Chong *et al.*, 2010). The concept of NIPC is shown in Figure 2.4a and 2.4b. The concentrating sunlight to the NIPC is similar to the non-imaging focusing heliostat, where the uniformity of illumination on receiver can be obtained from the superposition of the flat mirrors images which stack into one as shown in Figure 2.4b. The incident sunlight are reflected by the flat mirrors to the receiver, in which the size and shape of the illumination is nearly same to the CPV module.

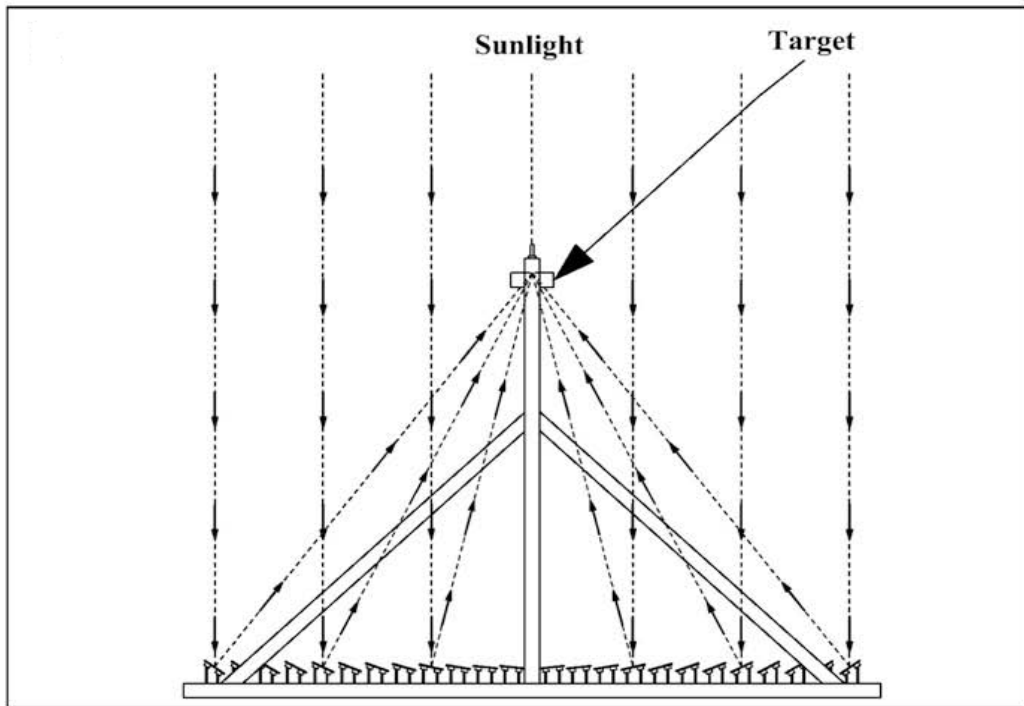
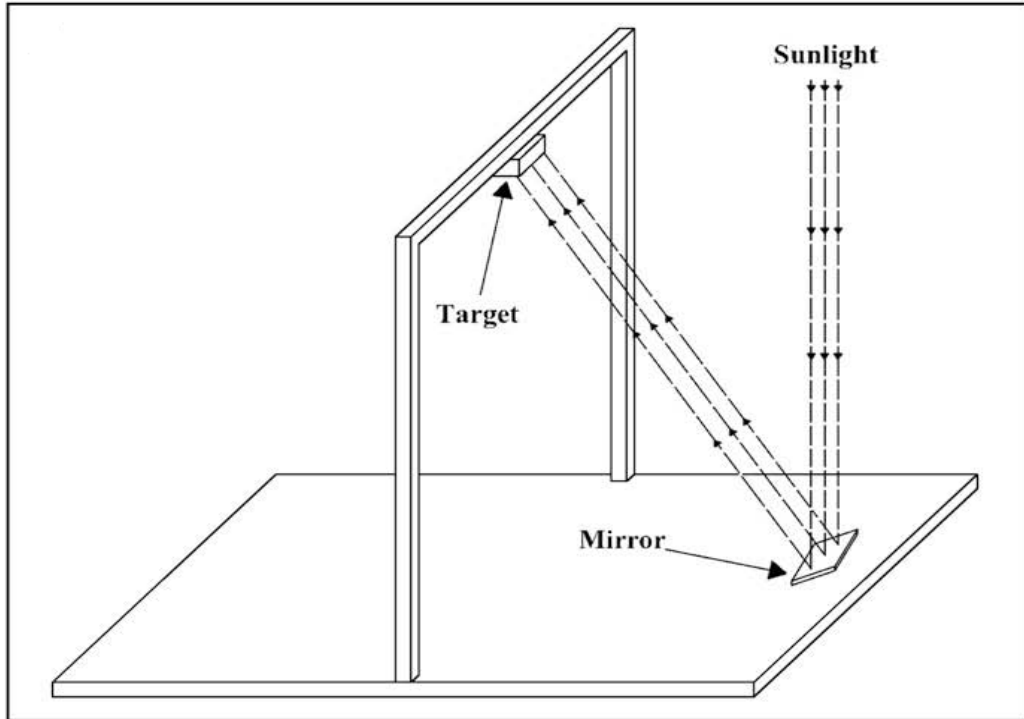


Figure 2.4: Conceptual layout of NIPC and Cross-sectional view of NIPC to show how the individual mirror directs the sunlight to the receiver, (a) isometric view, (b) side view (Chong *et al.*, 2009a).

2.2.2 Method of Sun Tracking

Currently, the two-axis sun-tracking method also known as azimuth-elevation (AE) method is implemented in the NIPC system for this study. The reflectors of the NIPC are mounted above the pedestal which allows the movements in azimuth axis and elevation axis. Movement of each axis is supplied by a fractional-horsepower motor through a gearbox drive. These motors receive signals from a central control computer that accurately track the sun position so that the reflectors normal intermediate between the sunray and the reflected rays which point toward the receiver. Figure 2.5 showed the schematic diagram of the setup of AE tracking method NIPC. From the diagram, the AA' axis is azimuth axis and BB' axis is elevation axis.

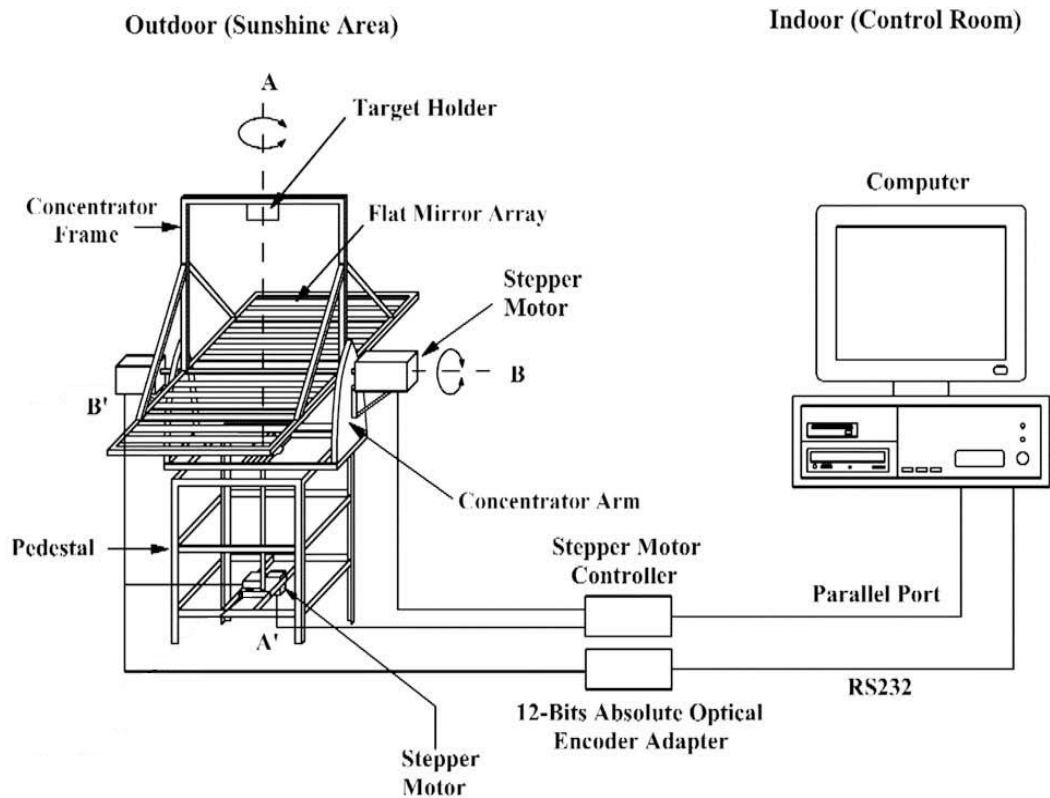


Figure 2.5: Schematic diagram of the setup of AE tracking method NIPC (Chong *et al.*, 2009a).

2.3 Automotive Radiator

Automotive radiator is a device of heat exchange to transfer heat energy from one medium to the environment. It consists a lot of parallel thin-wall tubes which allow water (medium of heat exchange) to pass through and the heat from the hot water is dissipated to the air stream which created by radiator's fan. The total heat transfer area of automotive radiator is typically high which contributed by the thin waved-shape fins sandwiched between the tubes. Most of the tubes and fins

are fabricated by metal which has high heat conductivity such as aluminum and copper to enhance the rate of heat conduction within tubes and fins. With higher rate of heat conduction, more heat energy can be dissipated to the environment. Therefore, automotive radiator has a very high heat transfer profile. In this study, automotive radiator is the key component which also the last stages of heat dissipation to the environment. Figure 2.6 shows the schematic diagram of an automotive radiator.

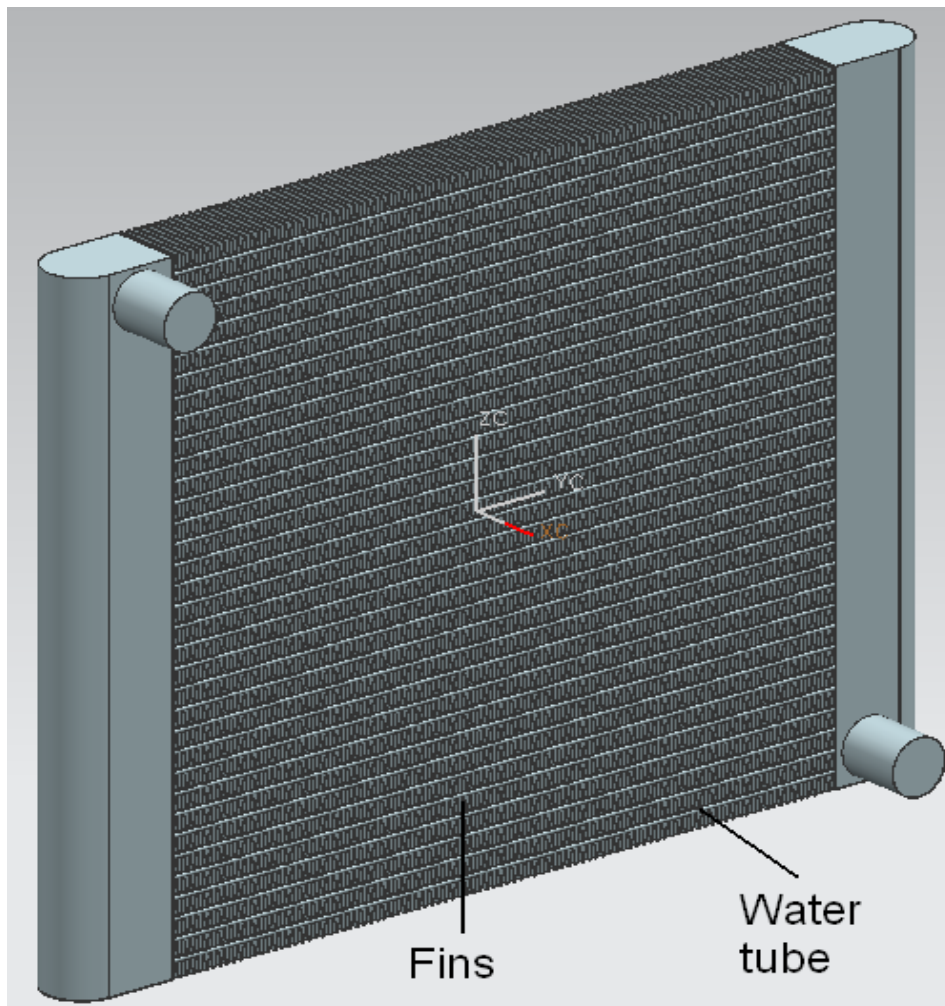


Figure 2.6: Schematic diagram of automotive radiator.

2.4 Cooling Tower

According to Cooling Technology Institute (2009), cooling tower is a heat rejection device which will extract the heat from water flow through it and dissipate to the atmosphere. The method of heat dissipation of cooling tower is evaporation. Small portion of water will be evaporated into the moving air stream created by cooling fan when the water flows through the cooling tower to provide effective cooling to the rest of water. The dissipated heat transferred to the air stream will raise the air's temperature and relative humidity and finally discharged to the atmosphere.

2.5 Heat Transfer

Heat transfer is a discipline of thermal engineering that concerns the exchange of heat from within two physical systems. The fundamental methods of heat transfer are classified into a few mechanisms, which are conduction, radiation, convection, and phase-change transfer. Since phase-change heat transfer is more complicated, it is not discussed here. Heat transfer occurs when there is a temperature-difference between two regions which have different temperature (Geankoplis, 2003).

Heat transfer methods are widely used in many engineering fields including automotive engineering, power plant engineering, insulation and else. Heat transfer is an important part of this study because automotive radiator used in the study is a heat exchange device. The rate of heat transfer within automotive radiator is also considered and calculated.

2.5.1 Conduction

Conduction is a mode of transfer of thermal energy within bodies of matter, due to a temperature gradient occurred within them. Conduction also defined as collisional and diffusive transfer of kinetic energy of particles of matter. Conduction takes place in all forms of matter such as solids, liquids and gases. In solids, it is due to the combination of vibrations of the molecules in a lattice or phonons with the energy transported by free electrons. In gases and liquids, conduction is due to the collisions and diffusion of the molecules during their random motion. In conduction, the heat flows through the body itself from higher temperature part to lower temperature until equilibrium is achieved. In the study, conduction is considered in the heat transfer within cooling block and also the heat transfer within automotive radiator's tubes and fins. The equation to calculate the rate of heat transfer of conduction is stated as:

$$\dot{Q} = \frac{kA\Delta T}{l} \quad (\text{W}) \quad (2.1)$$

Where k is the conductivity of material ($\text{Wm}^{-1}\text{K}^{-1}$), A is the cross-sectional surface area (m^2), ΔT is the temperature difference between two ends ($^{\circ}\text{C}$) and l is the length of heat transfer between two ends (m). (Çengel, 2003)

2.5.2 Radiation

Radiation is electromagnetic radiation generated by the thermal motion of charged particles in matter. All matter will emit thermal radiation with a temperature greater than absolute zero (Blundell and Blundell, 2006). Radiation also represents a conversion of thermal energy into electromagnetic energy. The characteristics of radiation depends on various properties of the surface it is emanating from, such as the temperature of it, its spectral absorptivity and spectral emissive power, as expressed by Kirchhoff's law (Blundell and Blundell, 2006). A radiating body is characterized as black body where the surface has perfect absorptivity and emissivity at all wavelengths. The radiation of such perfect emitters is called black-body radiation. The ratio of any body's emission relative to that of a black body is the body's emissivity, so that a black body has an emissivity of unity. Others radiating body which are not black body have emissivity which is less than 1. The equation to calculate the rate of heat transfer of radiation is stated as:

$$\dot{Q} = \varepsilon \sigma A (T_b^4 - T_{amb}^4) \quad (\text{W}) \quad (2.2)$$

Where ε is the material emissivity, σ is the Stefan–Boltzmann constant ($5.67 \times 10^{-8} \text{Wm}^{-2}\text{K}^{-4}$), A is the radiating surface area (m^2), T_b is the surface temperature of radiating body ($^{\circ}\text{C}$) and T_{amb} is the temperature of the environment ($^{\circ}\text{C}$) (Çengel, 2003).

2.5.3 Convection

Convection is the transfer of thermal energy from one medium to another by the movement of fluids whether the movement of fluid is forced by external medium or created by fluid itself. The presence of bulk motion of the fluid enhances the heat transfer rate between the fluid and the solid surface (Blundell and Blundell, 2006). Convective heat transfer actually is the combination of the effects of heat diffusion and heat transfer by bulk fluid flow a process technically termed heat advection. The process of transfer of thermal energy from a solid to a fluid or the reverse requires not only transfer of heat by bulk motion of the fluid, but also diffusion of heat through the still boundary layer next to the solid. Thus, this process with a moving fluid requires both diffusion and advection of heat can be defined as convection. Convection is usually the dominant form of heat transfer in liquids and gases. There are two types of convection which are natural convection and forced convection.

Natural convection is caused by buoyancy forces that result from the variation of density due to variations of temperature in the same fluid. When the fluid is in contact with a hot surface, the molecules at that volume will separate and scatter, causing the mass of fluid at that volume become less dense. Therefore, the fluid is displaced vertically or horizontally while the cooler fluid which is denser will sink. Thus the hotter volume transfers heat towards the cooler volume of that fluid.

Forced convection occurred when there are external sources such as pump, fan and other which will create fluid flow to force the fluid flowing over the hot surface to absorb the heat from it or in the reverse to supply heat to certain surface by hot water. Normally, forced convection has higher heat transfer rate compare to natural convection because forced convection has higher flow rate than natural convection. The heat transfer from automotive radiator to the environment in this study is a forced convection. The equation to calculate the rate of heat transfer of convection is stated as:

$$\dot{Q} = hA\Delta T \quad (\text{W}) \quad (2.3)$$

where h is the heat transfer coefficient ($\text{Wm}^{-2}\text{K}^{-1}$), A is the total heat transfer area of convection (m^2), ΔT is the temperature difference between the contact surface and fluid ($^{\circ}\text{C}$) (Çengel, 2003).

2.5.3.1 Heat Transfer Coefficient

In convection, heat transfer coefficient varying depends on the condition in the fluid boundary layer which affected by the motion of fluid, surface geometry, and an assortment of fluid thermodynamic and transport properties (Incropera *et al.*, 2007). Basically, heat transfer coefficient is in the function of Nusselt number (dimensionless number), fluid conductivity and diameter of pipe in pipe flow or length of plate in plate flow. Their relationship as stated below:

$$h = \frac{Nuk}{D_h} \quad (2.4a)$$

$$h = \frac{Nuk}{L} \quad (2.4b)$$

where Nu is the Nusselt (dimensionless), k is the conductivity of fluid ($\text{Wm}^{-1}\text{K}^{-1}$), D_h is the hydraulic diameter of pipe (m) and L is the length of plate (m). From the equation, heat transfer coefficient of convection is directly proportional to Nusselt number and fluid conductivity but inversely proportional to the diameter of pipe or length of plate. Therefore, the change of Nusselt number will immediately influence the value of heat transfer coefficient in order influence the rate of heat transfer (Çengel, 2003).

2.5.3.2 Nusselt Number

In convection, Nusselt number is varying depends on the conditions in the fluid boundary layer such as rate of fluid flow, fluids properties which influenced by its temperature and geometry of the boundary of fluid flow. Below are the relationships between nusselt number and its parameter:

$$Nu = f(D_h, Re, Pr) \quad (2.5a)$$

$$Nu = f(L, Re, Pr) \quad (2.5b)$$

The above equations implies that for a given geometry, the Nusselt number is in the function of Re, Pr and D_h in pipe flow or L in plate flow. If these three parameters are known, it could be used to calculate the value of Nusselt number. From equations above, Re is the Reynolds number which is dimensionless, Pr is the Prandtl number which also dimensionless and D_h is the diameter of pipe (m) in pipe flow and L is the length of plate (m) in plate flow. Nusselt number has several of correlation depends on different Reynolds number (laminar or turbulent), fluid flow boundary (pipe flow or plate flow) and value of Prandtl number (Incropera *et al.*, 2007).

2.5.3.3 Reynolds Number

Reynolds number is a dimensionless number which measure the ratio of inertial forces to viscous forces and quantify the relative importance of these two forces in a fluid flow. Therefore, Reynolds number is in a function of, fluid flow velocity, viscosity and dimension of fluid boundary. The relationships between Reynolds number and the parameters are stated below:

$$\text{Re} = \frac{\rho v D_h}{\mu} \quad (2.6a)$$

$$\text{Re} = \frac{\rho v L}{\mu} \quad (2.6b)$$

Where ρ is the density of fluid (kgm^{-3}), v is the velocity of fluid flow (ms^{-1}), μ is the dynamic viscosity (Nsm^{-2}) and D_h is the diameter of the pipe in pipe flow (m), L is the length of plate in plate flow. From equations above, Reynolds number is directly proportional to density and velocity of fluid and also the dimension of fluid boundary (diameter of pipe in pipe flow or length of plate in plate flow) but inversely proportional to dynamic viscosity of fluid. Reynolds number also classifies the fluid flows into laminar flow and turbulent flow.

2.6 Computational Fluid Dynamics (CFD)

Computational fluid dynamics (CFD) is a branch of fluid mechanics that applies numerical methods and algorithms to solve and analyze problems of fluid flows. High performance computers are required to perform all of the numerical calculations to obtain the interaction of fluids with defined surfaces in finite boundary conditions.

2.6.1 Standard K – epsilon Turbulent Model

The standard K-epsilon model is one of the widely used turbulence models of computational fluid dynamics used to construct a model to predict the turbulent effect of fluid flow.

Below are the governing equations of Standard K – ϵ turbulent model provided by Versteeg and Malalasekera (1995):

Continuity equation:

$$\frac{\partial \bar{\rho} \bar{u}_i}{\partial x_i} = 0 \quad (2.7a)$$

Momentum equation:

$$\bar{\rho} \bar{u}_j \frac{\partial \bar{u}_i}{\partial x_j} = -\frac{\partial \bar{p}}{\partial x_i} + \frac{\partial}{\partial x_i} \left[\bar{u}_i \left(\frac{\partial \bar{u}_i}{\partial x_j} + \frac{\partial \bar{u}_j}{\partial x_i} \right) \right] \quad (2.7b)$$

Energy equation:

$$\rho u_j \frac{\partial \bar{T}}{\partial x_j} = \frac{\partial}{\partial x_j} \left[\left(\frac{\mu_t}{\sigma_i} + \frac{\mu_t}{\sigma_t} \right) \frac{\partial \bar{T}}{\partial x_j} \right] \quad (2.7c)$$

Turbulent kinetic energy (k) equation:

$$\rho u_j \frac{\partial k}{\partial x_j} = \frac{\partial}{\partial x_i} \left(\frac{\mu_t}{\sigma_k} \frac{\partial k}{\partial x_j} \right) + \mu_t \left(\frac{\partial \bar{u}_i}{\partial x_j} + \frac{\partial \bar{u}_j}{\partial x_i} \right) \frac{\partial \bar{u}_i}{\partial x_j} - k \varepsilon \quad (2.7d)$$

Turbulent kinetic energy dissipation (ε) equation:

$$\rho u_j \frac{\partial \varepsilon}{\partial x_j} = \frac{\partial}{\partial x_i} \left(\frac{\mu_t}{\sigma_\varepsilon} \frac{\partial \varepsilon}{\partial x_j} \right) + C_1 \mu_t \frac{\varepsilon}{k} \left(\frac{\partial \bar{u}_i}{\partial x_j} + \frac{\partial \bar{u}_j}{\partial x_i} \right) \frac{\partial \bar{u}_i}{\partial x_j} - C_2 \rho \frac{\varepsilon^2}{k} \quad (2.7e)$$

The empirical constants in the above equations are given as: $C_1 = 1.44$, $C_2 = 1.92$,

$C_\mu = 0.09$, $\sigma_k = 1.0$, $\sigma_\varepsilon = 1.3$. Full description and calculation for these entire

empirical constant were provided by Rodi (1980).

CHAPTER 3

METHODOLOGY

3.1 Theoretical Study

The theoretical study on the automotive radiator cooling system has been carried out before the experimental data were collected. In this thesis, there are two theoretical studies, which are the theoretical study of the automotive radiator and the theoretical study of the cooling block. A three-dimensional (3-D) computational fluid dynamic (CFD) model is used to simulate the temperature at the central point (the hottest point) of the cooling block under various solar heat flux input, water mass flow rate and water inlet temperature to the cooling block. In the theoretical study, the heat rejection by the automotive radiator and cooling block was calculated by applying the formulas of heat transfer under different wind speeds, water flow rate and different surface areas of cooling. The objective of theoretical modeling for both the automotive radiator and cooling block is to finalise the design specification of the prototype cooling system such as wind speed and water flow rate (Chong and Tan, 2012). The details of theoretical studies are discussed below.

3.1.1 Theoretical Study of Heat Transfer of Automotive Radiator

According to Chong and Tan (2012), the heat rejection of automotive radiator is studied using analytical methods based on the case of forced convection by air and heat dissipation due to radiation. The heat rejection rate of radiator is the rate of radiator removing the excess heat from circulating cooling water to the environment. The automotive radiator has a total surface area of 3.8 m² in which only 2.2 m² of the surface area is covered by the fan. In the analysis of heat rejection, convection is only considered at the regions of the radiator where covered by the air-flow created by the fan while radiation is considered on all surface area of radiator. The heat transfer of the automotive radiator through conduction is small and can be ignored in the calculation. The forced convection and radiation are the main factors of heat transfer in the automotive radiator. The total heat removed by the automotive radiator is the summation of heat removed by both forced convection and radiation. The formula of the total heat removed by the automotive radiator can be calculated using formula (2.3) as shown below:

$$Q = hA\Delta T \quad (\text{W}) \quad (2.3)$$

Refer to the condition of heat transfer between environment and automotive radiator, Q is the heat rejection of automotive radiator through forced convection (W), h is the heat transfer coefficient ($\text{Wm}^{-2}\text{K}^{-1}$) of forced convection, A is the total heat transfer area of forced convection (m^2) stated as 2.2 m², ΔT is the temperature difference measured between the surface of radiator and air ($^{\circ}\text{C}$). The

heat transfer coefficient h can be calculated by using equation 2.4c:

$$h = \frac{Nu_a k_a}{D_h} \quad (2.4c)$$

where k_a is the thermal conductivity of air ($\text{Wm}^{-1}\text{K}^{-1}$) which depends on the temperature of environment, D_h (m) the hydraulic diameter which is defined as the effective diameter of a noncircular tubes in the first approximation, can be obtained as:

$$D_h = \frac{4A_c}{P} \quad (3.1)$$

in which A_c and P are the cross-sectional area, $6.914 \times 10^{-5} \text{ m}^2$, and the perimeter, 0.0723 m , of the radiator tubes respectively. Nu_a (dimensionless) is Nusselt number in the case of forced convection between the radiator surface and environment. Since the automotive radiator consists of an array of 33 non-circular tubes arranged in parallel from top to bottom and the wind created by fan flow across the parallel tubes, therefore, it is treated as a case of cross flow on a non-circular tube. Hence, the Reynolds number can be calculated by applying equation (2.6a) as shown below:

$$Re_D = \frac{\rho_a v_a D_h}{\mu_a} \quad (2.6a)$$

where Re_D (dimensionless) is the Reynold number in the case of forced convection between the radiator surface and the environment, ρ_a is the density of air (kgm^{-3}), v_a is the average wind speed of fan with 3 ms^{-1} and μ_a is the dynamic viscosity of air (Nsm^{-2}). The density and dynamic viscosity can vary dependent on the environment temperature. According to Zukauskas (1972), the Nusselt number of automotive

radiator for the case of cross flow on non-circular tubes can be expressed as

$$Nu_a = C Re_D^m Pr_a^n \left(\frac{Pr_a}{Pr_s} \right)^{1/4} \quad (3.2)$$

$$\left[\begin{array}{l} 0.7 \leq Pr_a \leq 500 \\ 1 \leq Re_D \leq 10^6 \end{array} \right]$$

where Pr is the Prandtl number. All the properties (ρ_a , μ_a , Pr_a , k_a) are evaluated based on the air temperature flowed across the radiator (same as ambient temperature) except Pr_s is evaluated based on radiator's surface temperature. These parameters' value can be obtained from Table A.4 of Incropera *et al.* (2007). According to Incropera *et al.* (2007), given that $n = 0.37$ for $Pr_a \leq 10$ and $m = 0.5$, $C = 0.51$ for Re_D in the range of 40-1000. With the Nusselt number, the heat transfer coefficient of forced convection between automotive radiator and the environment can be calculated as well the heat rejection rate of radiator (Chong and Tan, 2012)

For the heat transfer by radiation, the rate of heat transfer is stated below:

$$Q_{radiation} = \varepsilon \sigma A (T_s^4 - T_{amb}^4) \quad (2.2)$$

where ε is a property of radiative surface termed the emissivity of the surface with values from 0 to 1 depending on different surface finishing and material. Incropera *et al.* (2007) provided a list of emissivity for various materials. Since the automotive radiator is painted in black, therefore the surface emissivity of the whole radiator is stated as 0.98 (Incropera *et al.*, 2007). σ is the Stefan-Boltzmann constant equal to $5.67 \times 10^{-8} \text{ Wm}^{-2}\text{K}^{-4}$. A is the total surface area for heat transfer. T_s is the average temperature of radiative surface and T_{amb} is the ambient temperature (Chong and Tan, 2012).

3.1.2 Theoretical Study of Heat Transfer of Cooling Block

In this section, the theoretical study of heat transfer of cooling block is carried out by using analytical formulas for forced convection similar to the study of automotive radiator, the forced convection in cooling block is initiated by water (Chong and Tan, 2012). The heat power converted from excess solar flux is absorbed by back side of cooling block and then conducted to the finned surface which forced convection take part. The heat conduction within cooling is calculated by using equation 2.1:

$$Q = \frac{k_{cu} A \Delta T}{l} \quad (2.1)$$

where k_{cu} is the conductivity of the material of cooling block which is copper with the value of $387 \text{ Wm}^{-1}\text{K}^{-1}$, A is the cross-sectional surface area of heat conduction which is 0.01 m^2 , ΔT is the temperature difference measured between two ends of conduction ($^{\circ}\text{C}$) and l is the length of heat transfer between the two ends with 0.005 m . In the analysis, the heat loss from the cooling block's surfaces through radiation and natural convection are small and can be neglected in the calculation of heat transfer. Therefore, the heat conducted to the finned surface is considered equal to heat absorbed by the cooling water through forced convection. The cooling block's finned surface has a total surface area of 0.11922 m^2 , since forced convection is the main consideration of heat transfer in the study of cooling block, the heat transfer coefficient of forced convection applied between the cooling block and cooling water is given by equation 2.4b:

$$h = \frac{Nu_w k_w}{L} \quad (2.4b)$$

where k_w is the thermal conductivity of water ($\text{Wm}^{-1}\text{K}^{-1}$) which depends on its temperature, L is the length of water flow in the cooling block stated as 0.124 m, Nu_w (dimensionless) is Nusselt number in the case of forced convection between the finned surface of cooling block and water. Since the cooling block's inner is a flat plate with fins, therefore the flow type in the cooling block is consider as a plate flow. Hence, the Reynolds number can be calculated by applying equation (2.6b) as shown below:

$$\text{Re}_L = \frac{\rho_w v_w L}{\mu_w} \quad (2.6b)$$

where Re_L (dimensionless) is the Reynold number in the case of forced convection between the cooling block's finned surface and water, ρ_w is the density of water (kgm^{-3}), v_w is the average speed of water in the cooling block with 0.35 m/s and μ_w is the dynamic viscosity of water (Nsm^{-2}). The density and dynamic viscosity can vary dependent on the temperature of water. According to Incropera *et al.* (2007), the Nusselt number of convection between cooling block and water can be expressed as:

$$Nu_w = 0.453 \text{Re}_L^{1/2} \text{Pr}_w^{1/3} \quad (3.3)$$

all the properties (ρ_w , μ_w , Pr_w , k_w) are evaluated based on the temperature of water in the cooling block. These parameters can be obtained from table A.6 of Incropera *et al.* (2007). With the Nusselt number, the heat transfer coefficient of forced convection between cooling block and water can be calculated as well the heat transfer rate to the water (Chong and Tan, 2012).

3.2 Computational Fluid Dynamic Simulation of 3-D modeling Cooling Block

A Computational Fluid Dynamic (CFD) program is employed to perform a flow and heat transfer analysis to a specially designed cooling block for the dense array CPV system. The numerical modeling of the cooling block is illustrated in Figure 3.1 (Chong and Tan, 2012).

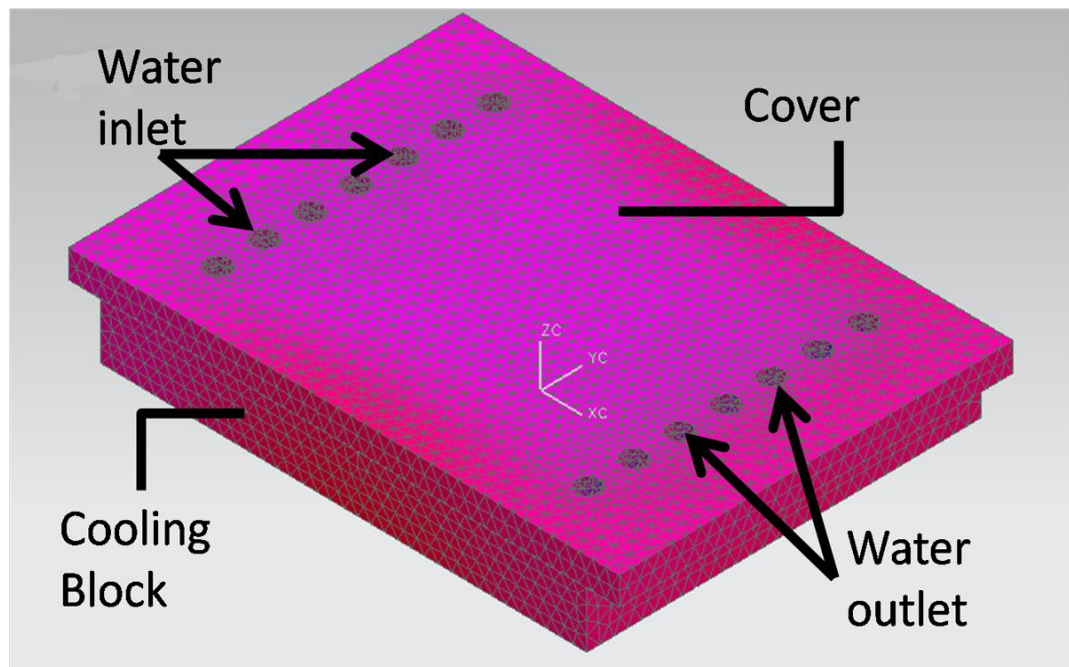


Figure 3.1: Drawing to show the numerical modeling of the cooling block where its domains comprises of three major parts of the cooling block with slot fins, cooling block cover and water acting as cooling fluid (Chong and Tan, 2012).

Its domains comprises of three major parts including cooling block with slot fins, cooling block cover and water acting as cooling fluid. These three parts

are meshed by tetrahedral meshing method into a total of 83,835 finite elements with spacing of 5 mm in size wherein 34,785 elements for the cooling block, 21,578 elements for the cover and 27,469 elements for the fluid. Furthermore, all the surfaces in contact within these three parts must be well defined. To start the iteration of simulation, the fluid inside the cooling block is assumed to have incompressible flow at the steady-state. The 3-D governing equations of mass, momentum, energy, turbulent kinetic energy and turbulent kinetic energy dissipation rate in the steady-state are listed as follow (Versteeg, 1995 and Malalasekera, 1995):

Continuity equation:

$$\frac{\partial \bar{\rho} \bar{u}_i}{\partial x_i} = 0 \quad (2.7a)$$

Momentum equation:

$$\bar{\rho} u_j \frac{\partial \bar{u}_i}{\partial x_j} = -\frac{\partial \bar{p}}{\partial x_i} + \frac{\partial}{\partial x_i} \left[\mu_t \left(\frac{\partial \bar{u}_i}{\partial x_j} + \frac{\partial \bar{u}_j}{\partial x_i} \right) \right] \quad (2.7b)$$

Energy equation:

$$\bar{\rho} u_j \frac{\partial \bar{T}}{\partial x_j} = \frac{\partial}{\partial x_j} \left[\left(\frac{\mu_t}{\sigma_i} + \frac{\mu_t}{\sigma_t} \right) \frac{\partial \bar{T}}{\partial x_j} \right] \quad (2.7c)$$

Turbulent kinetic energy (k) equation:

$$\bar{\rho} u_j \frac{\partial k}{\partial x_j} = \frac{\partial}{\partial x_i} \left(\frac{\mu_t}{\sigma_k} \frac{\partial k}{\partial x_j} \right) + \mu_t \left(\frac{\partial \bar{u}_i}{\partial x_j} + \frac{\partial \bar{u}_j}{\partial x_i} \right) \frac{\partial \bar{u}_i}{\partial x_j} - k \varepsilon \quad (2.7d)$$

Turbulent kinetic energy dissipation (ε) equation:

$$\bar{\rho} u_j \frac{\partial \varepsilon}{\partial x_j} = \frac{\partial}{\partial x_i} \left(\frac{\mu_t}{\sigma_\varepsilon} \frac{\partial \varepsilon}{\partial x_j} \right) + C_1 \mu_t \frac{\varepsilon}{k} \left(\frac{\partial \bar{u}_i}{\partial x_j} + \frac{\partial \bar{u}_j}{\partial x_i} \right) \frac{\partial \bar{u}_i}{\partial x_j} - C_2 \rho \frac{\varepsilon^2}{k} \quad (2.7e)$$

In this 3-D model simulation of cooling block, the *k-epsilon* turbulent model is employed which is being expressed based on equations (2.7a) to (2.7e). The empirical constants in the above equations are given as: $C_1 = 1.44$, $C_2 = 1.92$, $C_\mu = 0.09$, $\sigma_k = 1.0$, $\sigma_s = 1.3$. Full description and calculation for these entire empirical constant were provided by Rodi (1980). Generally, there are many turbulent models such as Reynolds Stress Model, large eddy simulation and etc. In the 3-D model simulation of cooling block, the standard *k-ε* turbulent model is employed. With the change of each parameter, 60 computational simulations are executed to obtain the temperature at the centre of cooling block that is the same location where the measurement is made in the experiment (Chong and Tan, 2012).

3.3 Experimental Setup

In the study, the experimental setup consists of two major components, which are the non-imaging planar concentrator (NIPC) and automotive radiator cooling system (Chong and Tan, 2012).

3.3.1 Construction of NIPC

A prototype of non-imaging planar concentrator (NIPC) has been designed and constructed to serve the purpose of tracking the sun and focusing the sunrays onto a target which is the copper cooling block installed on the target holder frame, just above the concentrating mirrors (Chong and Tan, 2012).

3.3.1.1 Specification of NIPC

The non-imaging planar concentrator has the capability to producing a good uniformity of solar illumination is consisted of 416 flat concentrating mirrors with $10\text{ cm} \times 10\text{ cm}$ each to form a total reflective area of 4.16 m^2 . These concentrating mirrors are array in a grid form with size of 21×21 as shown in Figure 3.2 (Chong and Tan, 2012).

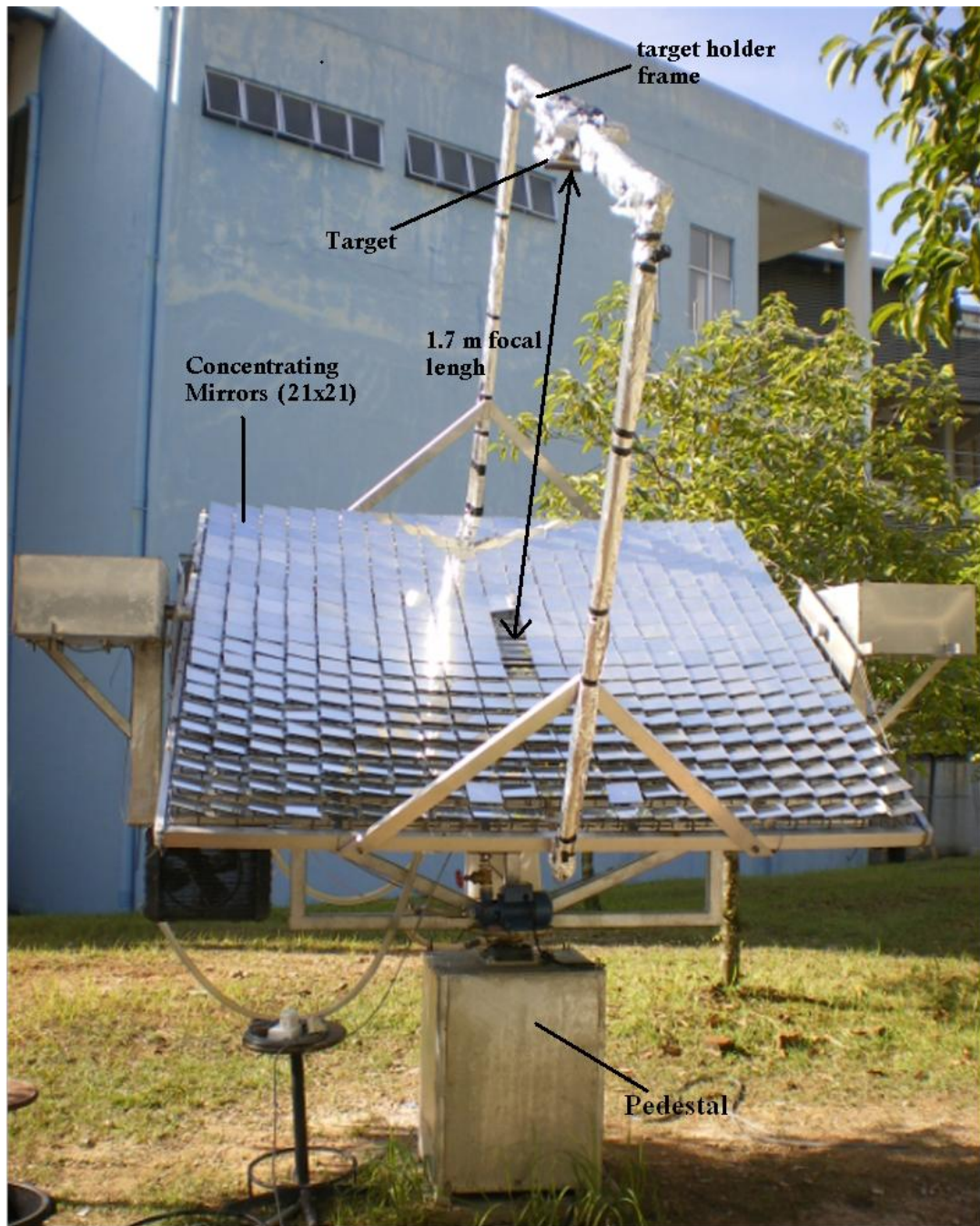


Figure 3.2: Picture to show the prototype of nonimaging planar concentrator that is located along the south-north orientation at latitude of 3.2° N and longitude of 107.7° E, in the campus of Universiti Tunku Abdul Rahman (UTAR), Kuala Lumpur, Malaysia (Chong and Tan, 2012).

From the diagram, the concentrating mirrors at the centre column which are installed exactly below the target holder frame have shadowing from the target holder frame and another 4 mirrors will be used to reflect light to active tracking sensor. Therefore, the 21 mirrors under the shadowing and 4 sensor mirrors were not considered and the final concentrating mirrors numbers are 416. According to Chong *et al.* (2009a, 2009b), to obtain optimum energy and concentration, the focal length should set close to 1.7 m if the 10 cm × 10 cm mirrors were arrayed in 21 × 21.

The mirrors holder frame and the target holder frame are made of Aluminum 6061 due to its light weight, therefore lower acting torque is required by the stepper motor to drive the concentrator (Chong and Tan, 2012). Other than that, the rest of non-imaging planar concentrator was made by mild steel which has higher strength than aluminum to serve the purpose of supporting the whole mirrors frame with the least deformation on it. The pedestal of the non-imaging planar concentrator is the supporting base which serves the purpose to support all the loads of the concentrator. The pedestal has similar function with columns or pillars in buildings which play an important role in supporting. Moreover, the pedestal also protects the azimuth stepper motor from rain which is installed inside it.

3.3.1.2 Tracking Method of NIPC

The active azimuth-elevation sun-tracking method has been adapted to the prototype of NIPC and each of the axes is driven by a stepper motor attached to worm gear reducer with gear ratio of 60. A Windows-based program implemented using Microsoft Visual Basic.net was developed to control the sun-tracking mechanism according to the day number of the year, the local time, time zone, latitude and longitude of the prototype installation as shown in Figure 3.3 (Chong and Tan, 2012).

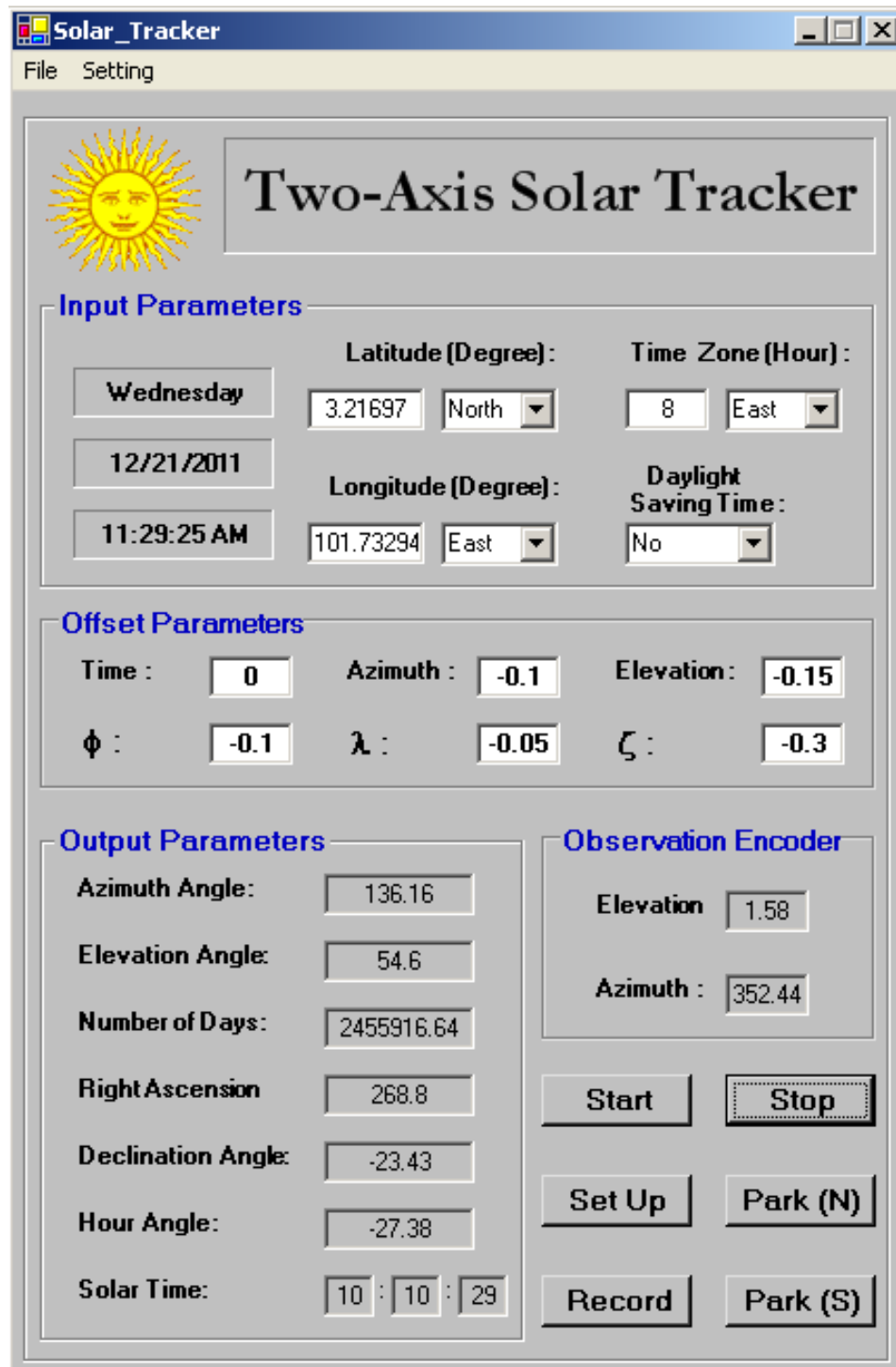


Figure 3.3: Windows-based program implemented using Microsoft Visual Basic.net developed to control the sun-tracking mechanism according to the day number of the year, the local time, time zone, latitude and longitude of the prototype installation (Chong and Tan, 2012).

The program acquires the aforementioned information for calculating the azimuth and elevation angles of the sun so that the stepper motors will be triggered to drive the concentrator frame to the required orientation (Chong *et al.*, 2009b, 2011). As the apparent position of the sun continue to change with time throughout the day, the computer will continuously send signals via the parallel port to the driver to adjust the orientation of concentrator frame appropriately about the azimuth and elevation axes for maintaining the tracking position. The tracker is commanded to follow the sun at all times because the program is run in repeated loops to ensure a smooth and continuous movement of the concentrator frame (Chong and Tan, 2012).

3.3.1.3 Flux Distribution of NIPC

In this section, solar flux distribution produced by the NIPC is discussed. The solar flux distribution casts on the cooling block was investigated via exposing a sand paper to the concentrated sunlight for a few seconds (Chong and Tan, 2012). Figure 3.4 show the concentrated sunlight has generated different grades of burnt mark on the sand paper.

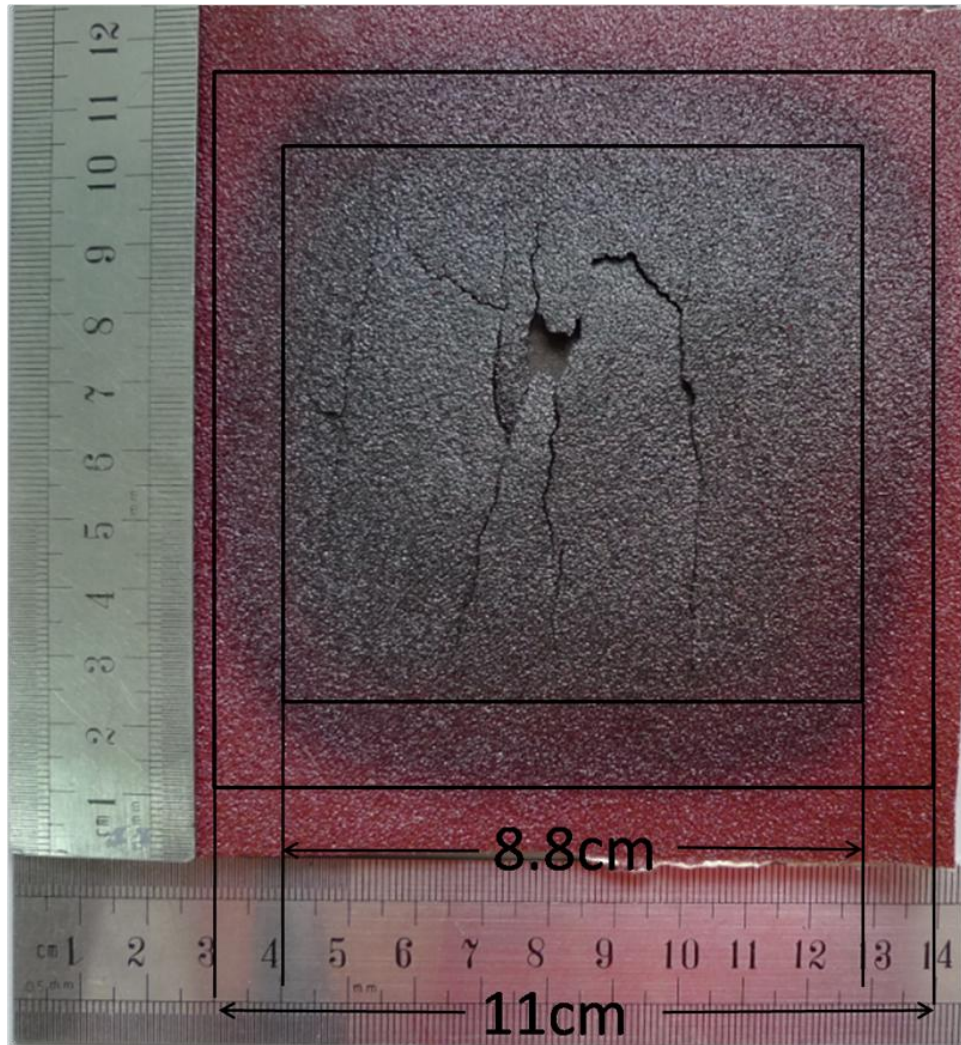


Figure 3.4: The concentrated sunlight has generated different grades of burnt mark on the sand paper, where the total area of burnt mark on the sand paper was measured as 11 cm \times 11 cm and a darker carbonized burnt area was measured as 8.8 cm \times 8.8 cm (Chong and Tan, 2012).

The total area of burnt mark on the sand paper was measured as 11 cm \times 11 cm and a darker carbonized burnt area was measured as 8.8 cm \times 8.8 cm (Chong and Tan, 2012). The solar flux distribution profile has been simulated according to

the dimension of prototype using ray-tracing method (Chong *et al.*, 2010). Figure 3.5 (a) and (b) show the simulated result in 3-D and 2-D plots accordingly in which the solar flux profile consists of a flat top area in the central region with maximum solar concentration ratio of 377 suns and it is named as uniform illumination area (Chong and Tan, 2012).

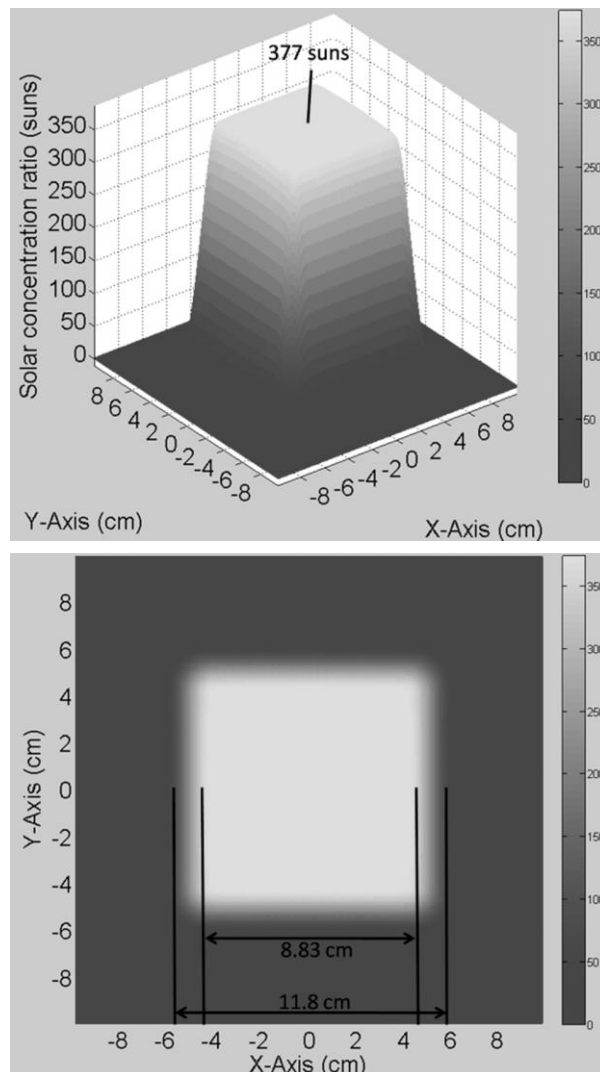


Figure 3.5: The simulation results of solar flux distribution for the prototype nonimaging planar concentrator that consisted of 420 flat mirrors in (a) 3-D and (b)

2-D plots with a focal distance of 170 cm (Chong and Tan, 2012).

The dimension of simulated result is reasonably close to the actual measurement, which is 11.8 cm × 11.8 cm in total area and 8.83 cm × 8.83 cm in the uniform illumination area (Chong and Tan, 2012).

3.3.2 Automotive Radiator Cooling System

The automotive radiator cooling system is another main component which plays an important role in cooling. It was sub-divided into four main parts, which are the automotive radiator, cooling block, water pump, and reservoir tank (Chong and Tan, 2012). Figure 3.6 shows the automotive radiator from a commercial automobile, “Proton Wira 1500 c.c.”.

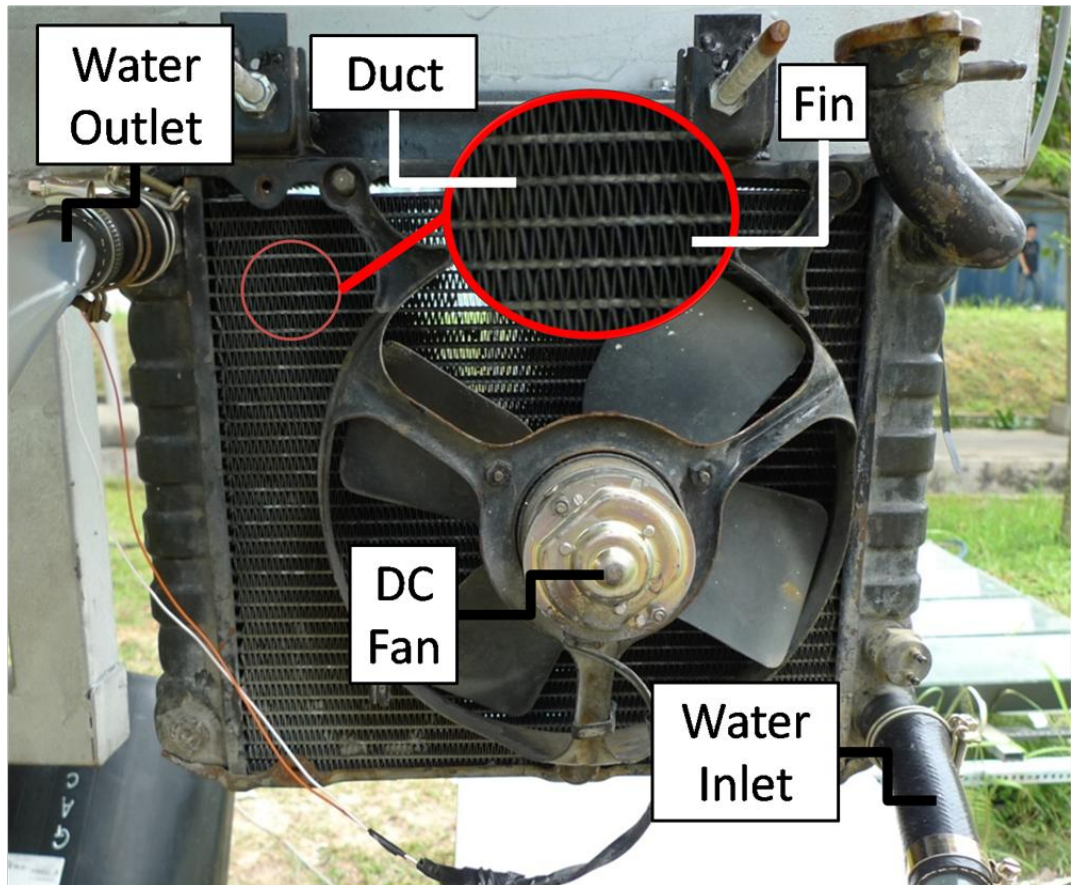


Figure 3.6: Picture to show the automotive radiator from a commercial automobile “Proton Wira 1500 c.c.” with the capacity of 1500 c.c to be used as the key device for the heat rejection in the cooling system (Chong and Tan, 2012).

This automotive radiator has 1500 c.c capacity has been used as the key device for the heat rejection in the cooling system. The materials of automotive radiator casing and tubes are aluminum alloy with high heat conductivity and light weight. It is easy to be installed into the prototype of NIPC with minimum load added to the driving motor especially the stepper motor of azimuth (Chong and Tan, 2012). From the diagram, the external fins with wavy shape were sandwiched

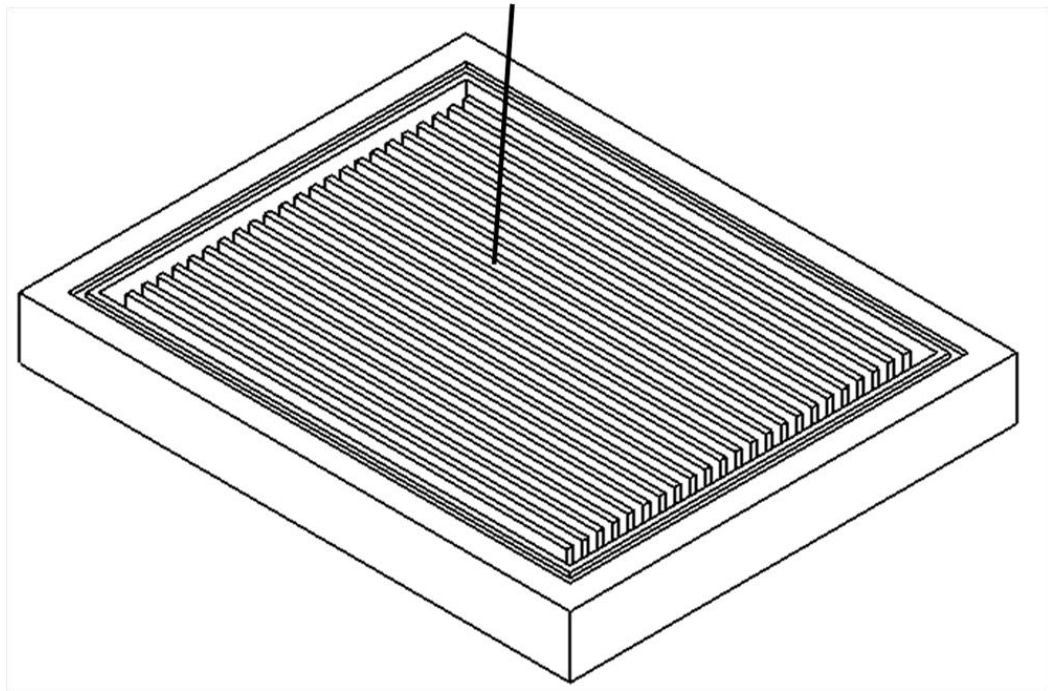
between the water ducts in the radiator are made of copper in order to have higher heat conductivity for increasing heat dissipation rate of radiator. The total heat transfer area of radiator is reasonably large, which includes the surface areas of radiator ducts and of copper fins. From measurement, the total surface area of radiator ducts is 0.8 m^2 and the total surface area of copper fins is 3 m^2 to result in 3.8 m^2 for the total surface area of radiator. A 280 mm diameter of DC fan with rated power of 50.6 W attached to the automotive radiator can create a significant air flow with the wind speed of 3 ms^{-1} . The Reynolds number Re_D for air flow across the radiator, Nusselt number Nu_a and heat transfer coefficient h are 730, 12 and $80 \text{ Wm}^{-2}\text{K}^{-1}$ using equation 2.6a, 3.2 and 2.4a respectively (Chong and Tan, 2012).

The cooling block is the heat sink for the dense-array CPV panel, which is the major component for absorbing and transferring the extra heat rejected by the dense-array CPV panel to the circulated cooling water. In this context, the preferred material of the cooling block is copper due to its high thermal conductivity which is about $387 \text{ Wm}^{-1}\text{K}^{-1}$ which allow the absorbed heat conducted with a faster rate to the finned-surface of cooling block in opposite side for rejecting the heat to cooling water by forced convection (Chong and Tan, 2012).

To ensure a high forced convection rate between the cooling block and water, the cooling block must have sufficient surface area that contacts with cooling

water. Therefore a copper block with a dimension $180\text{ mm} \times 146\text{ mm} \times 20\text{ mm}$ was machined into a shape with multiple water channels as shown in Figure 3.7 (Chong and Tan, 2012).

Multiple water channel pattern



180 mm x 146 mm x 20 mm

Figure 3.7: Drawing to show the cooling block made of copper with a dimension $180\text{ mm} \times 146\text{ mm} \times 20\text{ mm}$ to be machined into a pattern of multiple water channels (Chong and Tan, 2012).

The finned-surface of cooling block consisted multiple water channel pattern as shown in diagram above has contributed to a large surface area of

1192.20 cm² for the heat transfer between cooling block and water. Besides that, this pattern also allows water to pass through it with high speed by making use of the straight and narrow guides that increase the heat transfer coefficient of forced convection between cooling block and water. This cooling block is covered with an aluminum plate with a dimension of 204 mm × 146 mm × 10 mm to form a close system exactly same as Figure 3.1 (Chong and Tan, 2012).

In the experiment setup, an AC submersible water pump with model Nemo-100A and rated power of 100 W (Appendix B) is utilized for circulating the cooling water between the radiator and the cooling block. Its role is to create a constant water flow in whole automotive radiator cooling system with mass flow rate of 0.583 kgs⁻¹. The Reynolds number Re_L for water flow in the cooling block, Nusselt number Nu_w and heat transfer coefficient h are 31270, 192 and 1967 Wm⁻²K⁻¹ using equation 2.6b, 3.3 and 2.4b respectively (Chong and Tan, 2012).

Last but not least, the final component is a reservoir tank which acts as the start point and end point of the water circulation in the automotive radiator cooling system. It also provides additional space for storing back flow water when the system stops operation (Chong and Tan, 2012).

Figure 3.8 is the schematic diagram of the automotive radiator cooling system to show the flow direction of water in the experimental setup.

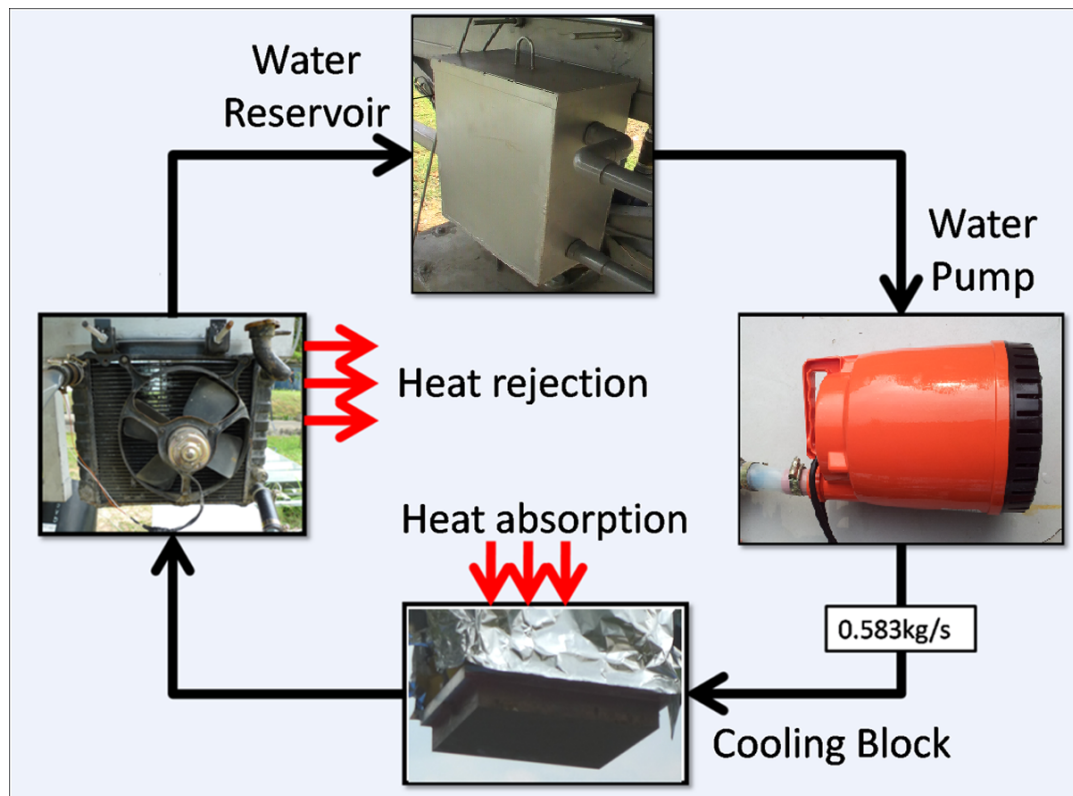


Figure 3.8: The schematic diagram to show all the components of the automotive radiator cooling system and the flow direction of water in the experimental setup (Chong and Tan, 2012).

After the water pump is switched on, the water from reservoir tank will flow to the copper cooling block located on top of the solar concentrator with the height of 2.2 m relative to the reservoir. When the water passes through the cooling block, it will absorb the thermal energy from the concentrated sunlight. The temperature of the water will rise after the heat absorption and the water will be heading to the automotive radiator which is located at 2.2 m below the cooling block. Inside the

automotive radiator, the water is forced through the parallel aluminum ducts evenly, in such a way that heat can be effectively dissipated during the process. In the radiator, the thermal energy carried by the water will be rejected to surrounding via forced convection created by the fan. The temperature of water will be decreased in the process of the heat rejection and then be circulated back to the reservoir tank so that a new circulation can be started again. Table 3.1 summarizes the specification of the whole experimental setup (Chong and Tan, 2012).

Table 3.1: The specification of experimental setup (Chong and Tan, 2012).

Radiator	
Radiator capacity	1500 c.c
Total surface area	3.8 m ²
Heat transfer area covered by fan, A	2.2 m ²
Cross section area of radiator ducts, A_c	6.914×10^{-5} m ²
Perimeter of radiator ducts, P	0.0773 m
Air flow boundary diameter (Fan's diameter)	280 mm
Wind speed created by fan, v_a	3 ms ⁻¹
Reynolds number of air across radiator, Re_D	730
Nusselt number of air, Nu_a	12
Heat transfer coefficient of air, h	80 Wm ⁻² K ⁻¹
Range of temperature for radiator surface, T_s	from 30 °C to 50 °C
Conductivity of radiator fin	387 Wm ⁻¹ K ⁻¹
Conductivity of radiator ducts	170 Wm ⁻¹ K ⁻¹
Rated power of fan	50.6 W
Cost of radiator with fan	USD 32.00
Cooling Block	
Dimension	180 mm × 146 mm × 20 mm
Number of slot-fins	23
Total surface area of each slot-fin	44.08 cm ²

Total heat transfer surface area	1192.20 cm ²
Conductivity	387 Wm ⁻¹ K ⁻¹
Water mass flow rate	0.583 kgs ⁻¹
Reynolds number of water, Re_L	31270
Nusselt number of water, Nu_w	192
Heat transfer coefficient of water, h	1967 Wm ⁻² K ⁻¹
Cost of cooling block	USD 90.00
Non-Imaging Planar Concentrator	
Total reflective area, A_r	4.2 m ²
Focal distance	1.70 m
Latitude	3.2°N
Longitude	107.7° E
Rated power of water pump	370 W
Total volume of water	12 liter
Cost of water pump	USD 38.00
Cost of water reservoir	USD 4.00

3.4 Data Collection and Experiments

On-site experimental data collection has been conducted for the automotive radiator cooling system to verify the feasibility of proposed cooling system. Furthermore, the conversion efficiency of concentrator photovoltaic module was measured under different operating temperature to justify the significance of cooling system in maintaining the good performance of CPV system (Chong and Tan, 2012).

To verify the theoretical modeling of automotive radiator cooling system, real-time data collection were conducted at the site and the measurement results were compared with the theoretical study. The experiments of data collection were

carried out in two sessions on two different days. For the experiments, all the measured parameters were closely monitored, such as Direct Normal Irradiance (DNI) ranging from 300 Wm^{-2} to 950 Wm^{-2} , stable ambient temperature ranging from $30 \text{ }^{\circ}\text{C}$ to $36 \text{ }^{\circ}\text{C}$, and stable air humidity ranging from 45 % to 72 %. Other parameters in the setting were ascertained to be the same in both experiments, which is wind speed of the fan is 3 ms^{-1} and mass flow rate of water is 0.583 kgs^{-1} (Chong and Tan, 2012).

First experiment was only conducted for 20 minutes wherein the data collection was performed for every minute. Second experiment was conducted for 6 hours from 10.30 a.m. to 4.30 p.m. where the data collection was performed for every interval of 15 minutes. During both data collections, the sun irradiance (DNI), water inlet temperature and outlet temperature of automotive radiator are collected. The collected data were then used to calculate the solar power input into the automotive radiator cooling system and heat rejection rate of the radiator. The DNI was measured by pyrliometer and the solar power input can be calculated using the following formula:

$$\mathbf{P}_{\text{in}} = \eta \times \text{DNI} \times A_r \quad (3.4)$$

where η ($= 0.8$) is the efficiency of direct conversion from solar energy to thermal energy considering the reflection loss of mirror and absorptivity of cooling block, A_r is the total reflective area of the prototype NIPC. The water inlet temperature and outlet temperature of automotive radiator are measured by thermometer and the

heat rejection rate of radiator can be computed from the following formula:

$$\dot{Q}_{out} = \dot{m} \times c \times \Delta T \quad (3.5)$$

where ΔT is the temperature difference of water between inlet and outlet of automotive radiator; \dot{m} is mass flow rate of water (0.583 kgs^{-1}) and c is heat capacity of water ($4200 \text{ J kg}^{-1}\text{K}^{-1}$) (Chong and Tan, 2012).

Apart from the data collection above, it is also important to know the performance of CPV module attached to the NIPC and proposed cooling system. As a result, a commercially available single CPV cell receiver module (Emcore, 2010) has been attached to the cooling block of the prototype NIPC and going to test its performance under high solar concentration. According to Figure 3.9, the left photo shows how the CPV module is attached on cooling block for on-site measurement and the right photo shows the CPV module exposed under high solar concentration during on-site measurement (Chong and Tan, 2012).

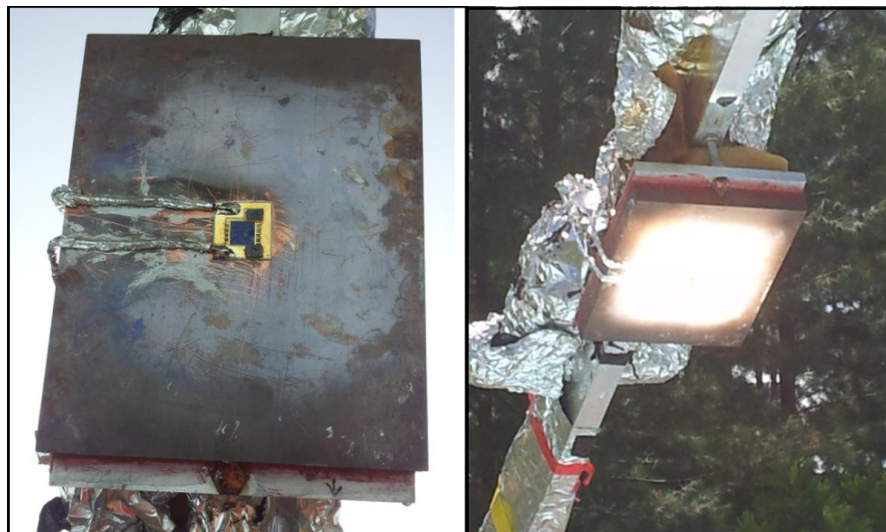


Figure 3.9: The left photo shows how the CPV module is attached on cooling block for on-site measurement and the right photo shows the CPV module exposed under high solar concentration during on-site measurement (Chong and Tan, 2012).

The electrical conversion efficiency of CPV module can be calculated using the formulas stated as follow:

$$\eta_{\text{CPV}} = (\mathbf{P}_{\text{CPV,out}}/\mathbf{P}_{\text{CPV,in}}) \times 100\% \quad (3.6)$$

where $\mathbf{P}_{\text{CPV,in}}$ is the solar power input received by the CPV module and $\mathbf{P}_{\text{CPV,out}}$ is the electrical power output generated by CPV module

$$\mathbf{P}_{\text{CPV,in}} = \eta \times \text{DNI} \times A_r \times (A_{\text{CPV}}/A_{\text{image}}) \quad (3.7)$$

$$\mathbf{P}_{\text{CPV,out}} = V_{\text{oc}} \times I_{\text{sc}} \times 0.87 \quad (3.8)$$

where A_{CPV} is the total active area of CPV cell ($1 \times 10^{-4} \text{ m}^2$), A_{image} is the total image area of the concentrated sunlight on the cooling block (0.01 m^2). V_{oc} is the measured open circuit voltage of CPV module and I_{sc} is the measured short circuit current of CPV module and 0.87 is the Fill Factor of CPV module provided by Emcore data sheet (2010). (Chong and Tan, 2012).

To calculate the temperature of CPV cell, the following formula is used:

$$T_{\text{CPV}} = (\mathbf{P}_{\text{CPV,in}} \times R_{\text{tot}} \times (1/A_{\text{CPV}}) \times (1 - \eta_{\text{CPV}})) + T_{\text{CB}} \quad (3.9)$$

where T_{CB} is the temperature of cooling block, R_{tot} is the total thermal resistance from cooling block to CPV cell consisted of the following materials: copper (cooling block), arctic silver thermal adhesive, copper layer in direct bond copper

(DBC) substrate, alumina layer in direct bond copper (DBC) substrate, copper layer in direct bond copper (DBC) substrate, solder material and CPV cell that can be calculated as:

$$R_{\text{tot}} = R_{\text{CPV}} + R_{\text{solder}} + R_{\text{DBC-copper}} + R_{\text{DBC-alumina}} + R_{\text{DBC-copper}} + R_{\text{arctic silver}} + R_{\text{copper}} \quad (3.10)$$

where

$$R_{\text{CPV}} = l_{\text{CPV}} / k_{\text{CPV}} \quad (3.11a)$$

$$R_{\text{solder}} = l_{\text{solder}} / k_{\text{solder}} \quad (3.11b)$$

$$R_{\text{DBC-copper}} = l_{\text{DBC-copper}} / k_{\text{DBC-copper}} \quad (3.11c)$$

$$R_{\text{DBC-alumina}} = l_{\text{DBC-alumina}} / k_{\text{DBC-alumina}} \quad (3.11d)$$

$$R_{\text{arctic silver}} = l_{\text{arctic silver}} / k_{\text{arctic silver}} \quad (3.11e)$$

$$R_{\text{copper}} = l_{\text{copper}} / k_{\text{copper}} \quad (3.11f)$$

where, l_{CPV} , l_{solder} , $l_{\text{DBC-copper}}$, $l_{\text{DBC-alumina}}$, $l_{\text{arctic silver}}$, and l_{copper} were the thicknesses of different materials measured as 0.12 mm, 0.15 mm, 0.3 mm, 0.635 mm, 0.1 mm and 5 mm respectively; k_{CPV} , k_{solder} , $k_{\text{DBC-copper}}$, $k_{\text{DBC-alumina}}$, $k_{\text{arctic silver}}$, and k_{copper} are referred as the thermal conductivity of different materials with values $55 \text{ Wm}^{-1}\text{K}^{-1}$, $29 \text{ Wm}^{-1}\text{K}^{-1}$, $400 \text{ Wm}^{-1}\text{K}^{-1}$, $24 \text{ Wm}^{-1}\text{K}^{-1}$, $7.5 \text{ Wm}^{-1}\text{K}^{-1}$ and $400 \text{ Wm}^{-1}\text{K}^{-1}$ respectively, which are provided by Luque and Andreev (2007).

(Chong and Tan, 2012).

CHAPTER 4

RESULTS and DISCUSSIONS

4.1 Results of Theoretical Study

The results of theoretical study consists two parts which are theoretical study of automotive radiator and theoretical study of copper cooling block. With these theoretical results, it could help us in deciding the final design specification of the prototype cooling system.

4.1.1 Result of theoretical study of automotive radiator

From Figure 4.1, result of theoretical study of automotive radiator shows the change of heat rejection rate by automotive radiator in the function of temperature difference between the radiator and ambient for wind speeds at 2 ms^{-1} and 3 ms^{-1} across the radiator provided that the heat transfer surface area are 2 m^2 , 2.2 m^2 and 2.4 m^2 (Chong and Tan, 2012).

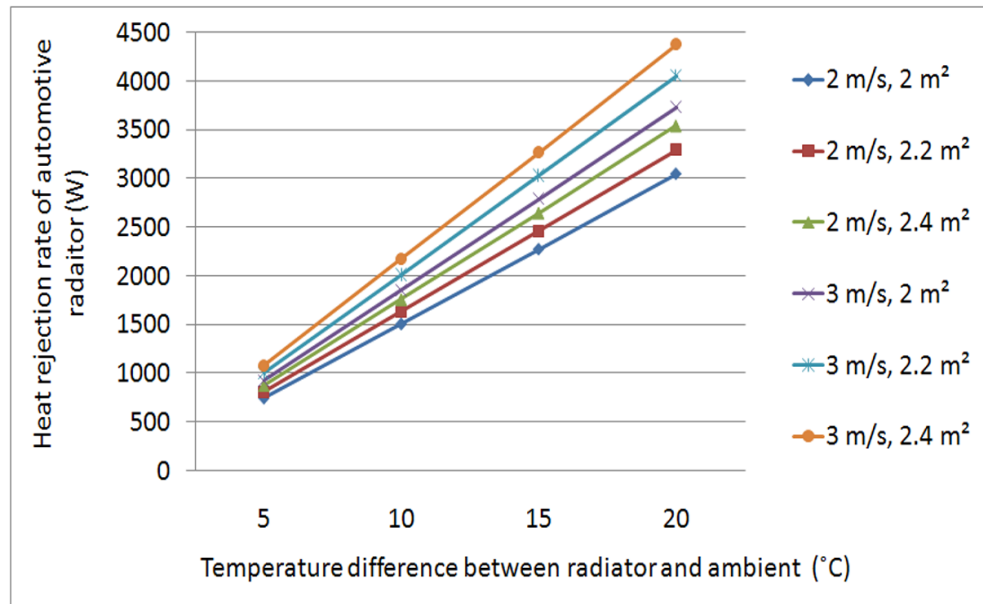


Figure 4.1: The graphs of heat rejection rate of automotive radiator versus temperature difference between radiator and ambient for different wind speeds and the heat transfer area of radiator (Chong and Tan, 2012).

From the graph, the heat rejection rate by the radiator has a linear relationship with the temperature difference between radiator and ambient environment. A higher temperature difference leading to a higher heat rejection rate fulfills the expression in equation (2.2) and equation (2.3). From Figure 4.1, the slope of graph for heat rejection rate versus temperature difference increases with the increase of wind speed and heat transfer area which means that the higher the wind speed and heat transfer area the higher the heat transfer co-efficient will be (Chong and Tan, 2012).

Estimate the direct normal irradiance (DNI) is 900 Wm^{-2} , the solar power input will be around 3000W calculated by using equation (3.4) $P_{in} = \eta \times \text{DNI} \times A_r$. From the chart, select the specification of the proposed cooling system's automotive radiator (which is the wind speed is 3 ms^{-1} and the heat transfer area is 2.2 m^2), when the temperature difference between radiator and the environment is $15 \text{ }^\circ\text{C}$, (which estimate the surface temperature of radiator is $50 \text{ }^\circ\text{C}$ and temperature of environment is $35 \text{ }^\circ\text{C}$), the automotive radiator is able to dissipate the heat power which is same amount with the solar power input. As a conclusion, with this specification of the chosen automotive radiator, is pretty capable to remove the excess heat power which is same amount with the solar power input as stated above. To verify the performance of the chosen automotive radiator, the real-time data collections will be conducted (Chong and Tan, 2012).

4.1.2 Result of Theoretical Study of Cooling Block

From Figure 4.2, result of theoretical study of cooling block shows the change of temperature at the center of cooling block as the function of solar heat flux input for different water inlet temperatures to the cooling block which are $30 \text{ }^\circ\text{C}$, $40 \text{ }^\circ\text{C}$ and $50 \text{ }^\circ\text{C}$ and different mass flow rates, 0.4 kgs^{-1} and 0.583 kgs^{-1} (Chong and Tan, 2012).

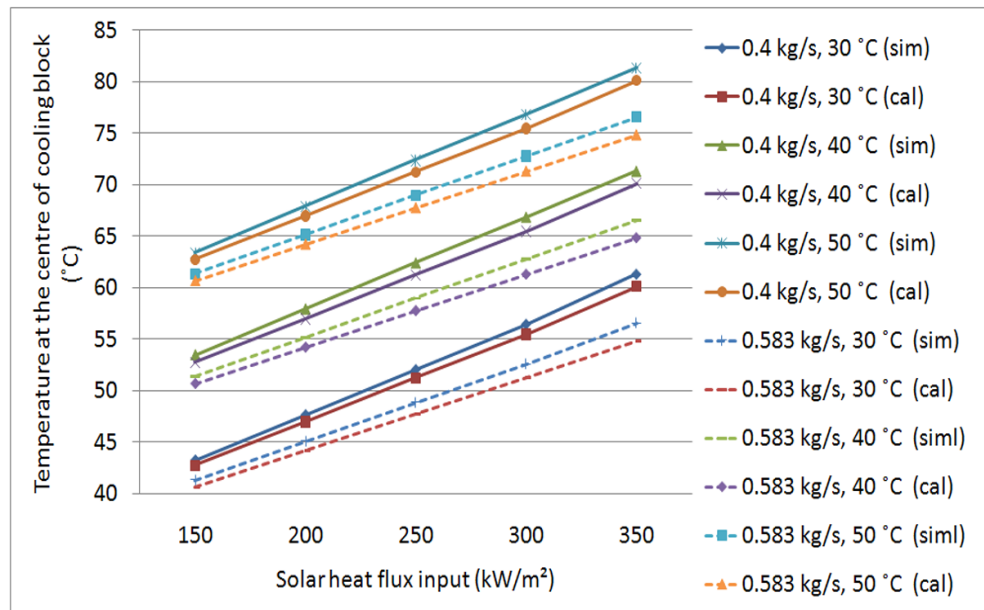


Figure 4.2: The graphs of temperature at the center of cooling block versus solar heat flux input for different water inlet temperature and mass flow rate. (Solid line represents mass flow rate of 0.4 kg s^{-1} and dot line represents mass flow rate of 0.583 kg s^{-1}) (Chong and Tan, 2012).

From the graphs, the rise in the water inlet temperature to the cooling block can cause the temperature of cooling block to rise for any particular value of solar heat flux input. It is because water with a higher inlet temperature carries more thermal energy than that of lower inlet temperature and hence reduces the temperature difference between cooling block and water. It has subsequently increased the thermal resistance for the heat dissipation from cooling block to water. From the graphs, the temperature of cooling block can be decreased by increasing the water mass flow rate at any specific solar heat flux input. A higher water mass flow rate can lead to a higher water speed profile, which subsequently increases the

heat transfer coefficient of convection between cooling block and water for dissipating more heat (Chong and Tan, 2012). As a result, a higher water mass flow rate is preferred.

From the graph, select the mass flow rate of the proposed cooling system which is 0.583 kgs^{-1} , consider the water inlet temperature is always around $30 \text{ }^\circ\text{C}$ and solar heat flux input to the cooling block is 300 kWm^{-2} , the temperature at the centre of cooling block (hottest point of cooling block) is about $50 \text{ }^\circ\text{C}$. As a conclusion, with this specification (water mass flow rate is 0.583 kgs^{-1}), the cooling block is capable to absorb the excess heat power and transfer to the cooling water to maintain the cooling block's temperature low. The verification of the performance of the cooling block is stated in the results of real-time data collections.

Figure 4.2 also shows a comparison between the simulated and calculated results. From the comparison, the simulated results are always slightly higher in the temperature of cooling block compared to that of the calculated results. The average error between the calculated and simulated results is about 1.86 % based on the following equation

$$error = \frac{T_{sim} - T_{cal}}{T_{cal}} \times 100\% \quad (4.1)$$

where T_{sim} is the temperature of cooling block obtained from the simulated result and T_{cal} is the temperature of cooling block obtained from the calculated result

(Chong and Tan, 2012).

4.2 Result of Data Collection and Experiment

The results of data collection are to verify the theoretical modeling of the automotive radiator cooling system. It consists of two real-time data collections, comparison between theoretical result and experimental result and also the CPV module conversion efficiency.

4.2.1 Real-time Data Collection

The Real time data collection consists of two sessions in two different days. First data collection was only conducted for 20 minutes with each data collected in every minute. Second data collection was conducted for 6 hours with each data collected in an interval of 15 minutes. The graphs for both data collections are plotted as shown below.

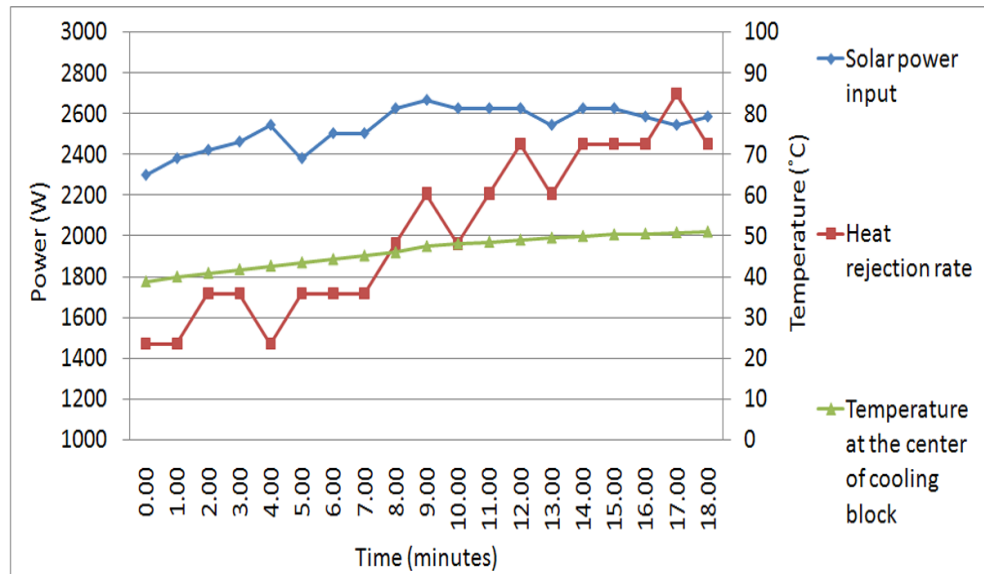


Figure 4.3: The graphs of solar power input, heat rejection rate and the temperature at the center of cooling block versus time (minutes) in the first experiment (Chong and Tan, 2012).

In Figure 4.3, solar power input, heat rejection rate and the temperature at the center of cooling block are plotted versus time (minutes) for the first experiment. From the graphs, the solar power input is reasonably constant throughout the experiment ranging from 2300 W to 2700 W, whilst the heat rejection rate of the radiator increases gradually over time until it reaches about 2400W. The heat rejection rate saturates in between 2400 W to 2700 W after 14 minutes of operation (Chong and Tan, 2012). On 17 minutes, the heat rejection rate of radiator is higher than the solar power input due to wind blows on the surface of radiator. This will cause the radiator's surface temperature dropped. According to equation (2.3), radiator's heat rejection rate will increase by increasing temperature

different between radiator's surface and environment. On the other hand, the temperature at the center of cooling block increases gradually in the beginning and then saturates at about 50°C after 14 minutes. From the observation, the automotive radiator is capable of removing the equal amount of heat as that of being absorbed by the cooling block thus reaching thermal equilibrium in the same period of time. In principle, it is plausible that the radiator has the capacity to remove heat at the rate of 2640 W or higher that is sufficient to equalize the solar power input if the temperature difference between radiator and ambient has achieved 15°C or higher (or the water temperature of cooling system of 50°C and the ambient temperature of 30-35°C) given that $h = 80 \text{ Wm}^{-2}\text{K}^{-1}$ and $A = 2.2 \text{ m}^2$ (Chong and Tan, 2012).

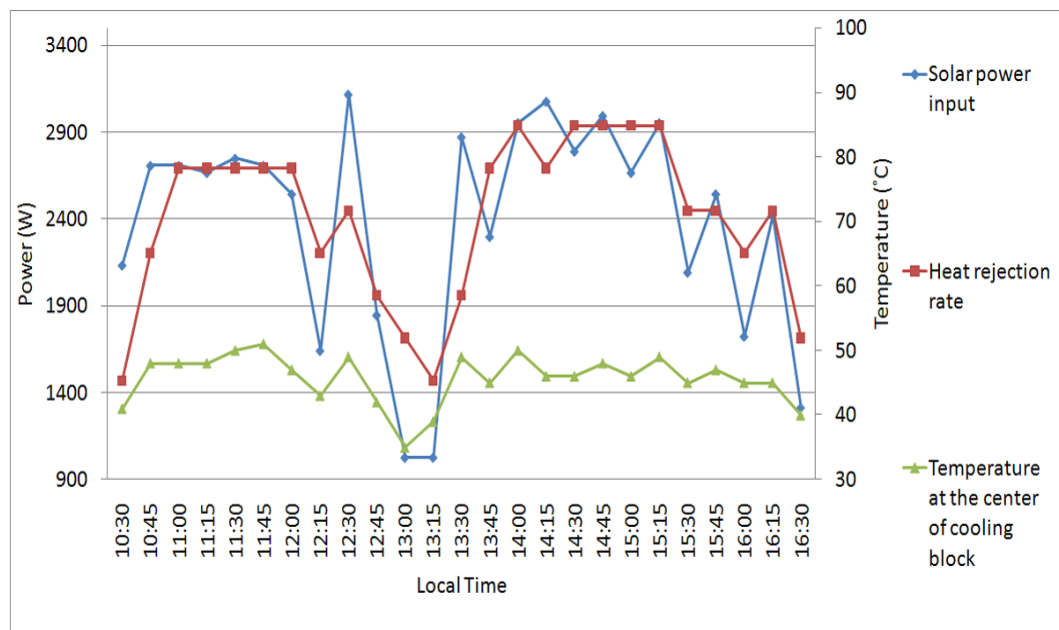


Figure 4.4: The graphs of solar power input, heat rejection rate and the temperature at the center of cooling block versus local clock time for a period of 6 hours at the

interval of 15 minutes in the second experiment (Chong and Tan, 2012).

Figure 4.4 shows the recorded results of the second experiment for a period of 6 hours at an interval of 15 minutes. Referring to Figure 4.4, the changes of the graphs can be viewed in four different periods of time, which are 1030 h – 1200 h, 1200 h – 1345 h, 1345 h – 1515 h, and 1515 h – 1630 h. From 1030 h to 1200 h, the solar power input increased from 2133W to 2708 W in the first 15 minutes and then maintained within the range 2544 W to 2749 W. In this period of time, the heat rejection rate during the first half an hour from 1469 W to 2693 W to equalize the solar input power and after that it maintained at the rate of 2693 W until 1200 h. The temperature at the center of cooling block maintained in the range of 47 °C to 51 °C throughout this period which is quite stable. From 1200 h to 1345 h, the solar power input fluctuated drastically within the range 1025 W to 3118 W caused by the intermittent sunlight. Consequently, the heat rejection rate and temperature at the center of cooling block also followed to fluctuate accordingly in the range of 1469 W to 2693 W and 35 °C to 49 °C respectively. From 1345 h to 1515 h, the solar power input was returned back to a stable condition again, which is in the range from 2298 W to 3077 W. For this period of time, the heat rejection rate and the temperature of cooling block were maintained stably in the range of 2693 W to 2938 W and 45 °C to 50 °C respectively. From 1515 h to 1630 h, the solar power input again has dramatic fluctuation within the range of 1313 W to 2954 W in a decreasing trend. The resulted heat rejection rate and temperature of cooling block

were then decreased ranging from 2938 W to 1714 W and from 49 °C to 40 °C respectively to follow the decreasing trend of solar power input. From the observation, the automotive radiator is capable to remove the absorbed heat and maintain the maximum temperature of cooling block well below 50 °C even though the experiment was continued for six hours. As a conclusion, the proposed automotive radiator cooling system with specification of 3 ms⁻¹ wind speed, 2.2 m² heat transfer area and 0.583kgs⁻¹ water mass flow is capable to remove the excess heat which is same amount with the solar power input and keep the temperature of cooling block low. These real-time data collections have verified the theoretical studies for both automotive radiator and cooling block (Chong and Tan, 2012).

4.2.2 Comparison between Theoretical Result and Experimental Result

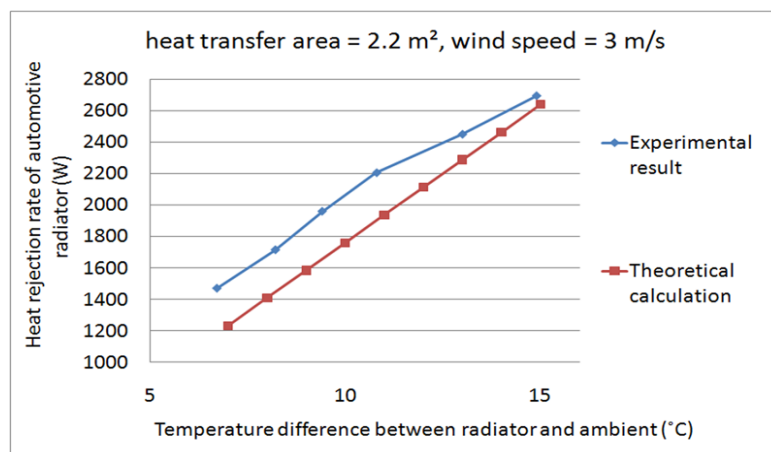


Figure 4.5: The graphs to show a comparison for the heat rejection rate of radiator between experimental and theoretical results (Chong and Tan, 2012).

By comparing the heat rejection rate of automotive radiator between the experimental and theoretical results as shown in Figure 4.5, the heat rejection rate of experimental result is slightly higher than that of theoretical result because there are other sources for the heat lost including conduction, natural convection and radiation throughout the cooling system. The heat rejection rate for the theoretical result is 91% of the experimental result (Chong and Tan, 2012).

4.2.3 CPV Module Conversion Efficiency

After the data collection, it is important to understand the effect of the proposed cooling system to the electrical conversion efficiency of the CPV module. As a result, a commercially available single CPV cell receiver module (Emcore, 2010) has been tested on the prototype NIPC (Chong and Tan, 2012).

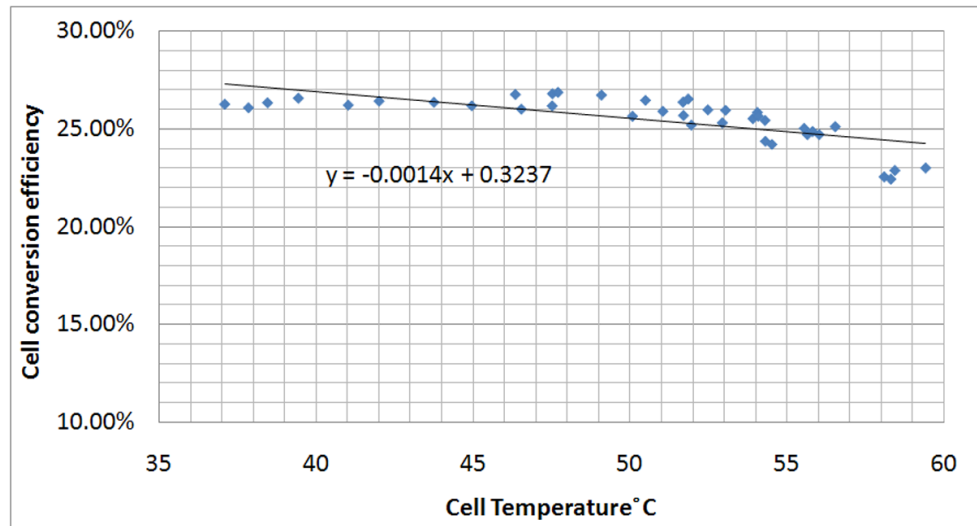


Figure 4.6: Graph to show the measurement result of electrical conversion efficiency of CPV module versus CPV cell temperature (Chong and Tan, 2012).

Figure 4.6 shows the measurement result of electrical conversion efficiency of CPV module versus CPV cell temperatures. The conversion efficiency is of a linear relationship to the cell temperature where the slope of the graph is -0.0014 which means the conversion efficiency reduced by 0.14 % for every increment of 1 °C. Referring to the graph, the maximum conversion efficiency is 26.85 % at the temperature 47.7 °C, whereas the lowest conversion efficiency is 22.39 % at the temperature 58.3°C (Chong and Tan, 2012).

There are two possible cases: (1) both water pump and fan are switched on in which the CPV cell temperature is 47.5 °C and the resultant conversion efficiency is 26.16 %; (2) water pump is switched on but the fan is off in which the CPV cell temperature is raised to 58.08 °C and the resultant conversion efficiency

is reduced to 22.51 %. For the case (1), the electrical output power produced by CPV at conversion efficiency of 26.16 % is 696.5 W provided that the DNI 800 Wm^{-2} and the resulted solar power input 2662.4 W. The net electrical power output will be 545.9 W after subtracting by 150.6 W consumed by both the fan and water pump. For the case (2), the electrical output power produced by CPV at conversion efficiency of 22.51 % is 599.3 W provided that the DNI 800 Wm^{-2} and the resulted solar power input 2662.4 W. The net electrical power output will be 499.3 W after subtracting by 100 W consumed by the water pump only. Comparing the two cases, the first case with the fan on can produce 46.6 W more net power output than the second case without the fan. Hence, we can conclude that efficient cooling system is very significant for CPV system to produce more net electrical power output. From Figure 4.4, the highest solar power input is 3118.7 W and therefore the net electrical power output can be as high as 665.3 W provided that the conversion efficiency is 26.16 %. (Chong and Tan, 2012).

4.3 Comparison of Automotive Radiator Cooling System to Cooling Tower

The comparison between automotive radiator cooling system and small size cooling tower are made in this part as shown in Table 4.1.

Table 4.1: Comparison between automotive radiator cooling system and small size cooling tower

	Automotive radiator	Small size cooling tower
Installation	Direct attached on NIPC and move together with NIPC.	Must be fixed on ground.
Size	430 mm × 330 mm × 5 mm (From measurement).	700mm diameter × 1130mm height (Jinling Refrigeration, 2009).
Dry weight	4 kg (From measurement).	38 kg (Jinling Refrigeration, 2009).
Flexible pipe usage	Shorter flexible pipes are required to connect the entire cooling system.	Longer flexible pipes are required to connect the entire cooling system.
Cooling capacity	1000 W to 4000 W, according to Fig. 4.1.	17500 W, according to calculation using eqn. (3.5) with specifications from Jinling Refrigeration (2009).
Parasitic load	50 W from cooling fan (from measurement) and 100 W from water pump (Appendix B).	180 W from cooling fan (Jinling Refrigeration, 2009) and 370 W from water pump (Appendix C).

From the result of comparison, automotive radiator is chosen as the main heat dissipation device for the introduced cooling system of the prototype NIPC

rather than small size cooling tower due to automotive radiator cooling system is more cost effective compare to small size cooling tower.

Compare both of the cooling devices, installation of automotive radiator is easier, it is because automotive radiator can move along with the prototype NIPC by just attached it on the prototype NIPC due to its size is smaller and lighter weight than cooling tower. Since automotive radiator can direct attached on prototype NIPC and move together with prototype NIPC, shorter flexible pipes are required to connect the entire cooling system. Since cooling tower is larger and heavier compare to automotive radiator, therefore it must be fixed on the ground and required longer flexible pipes to connect the entire cooling system.

By comparing the cooling capacity for both cooling devices, automotive radiator cooling system has lower cooling capacity than cooling tower. According to Figure 4.1, the chosen automotive radiator's (with 3 m/s wind speed and 2.2 m² heat transfer area) heat rejection rate is between 1000 W to 4000 W with temperature difference ranged from 5 °C to 20 °C, while the heat rejection rate for the smallest cooling tower is around 17500 W which calculated using equation (3.5):

$$\dot{Q}_{out} = \dot{m} \times c \times \Delta T \quad (3.5)$$

where \dot{m} is the mass flow rate of water equal to 3Th⁻¹ (Jinling Refrigeration, 2009) also equal to 0.833 kgs⁻¹, c is the water heat capacity (4200 J kg⁻¹K⁻¹) and ΔT is the

temperature difference with 5 °C provided by the data sheet (Jinling Refrigeration, 2009).

According to the design specifications of the prototype NIPC, the maximum solar power input is 3160 W which calculated by using equation (3.4):

$$P_{in} = \eta \times DNI \times A_r \quad (3.4)$$

Where η is 0.8, A_r is 4.16 m², and consider the DNI measured by pyrheliometer is maximum which is around 950 Wm⁻².

Refer to Figure 4.6, the concentrated photovoltaic (CPV) module has average conversion efficiency around 25 % of solar power input, the remaining 75 % will be converted to thermal energy which is about 2370 W. Therefore, the design specification of the heat dissipation rate for the cooling system must be equal or higher than 2370 W. According to the statements above, both systems have the heat dissipation rate higher than 2370 W.

Moreover, the parasitic energy consumption of the solar power concentrator must be kept as low as possible to maximize the power output from the system. Compare both automotive radiator and cooling tower's parasitic load, the minimum power consumption of the smallest cooling tower is 550 W which are 180W from the cooling fan (Jinling Refrigeration, 2009) and 370W from a

centrifugal pump (Appendix C) while the power consumption of the automotive radiator cooling system is 150W which are 50W from the cooling fan (from measurement) and 100W (Appendix B) from the submersible water pump.

According to the comparison above, although automotive radiator has lower heat dissipation rate than cooling tower, but its heat dissipation rate is higher than 2370 W which is the power input of NIPC, therefore the automotive radiator is suitable to use as a cooling device for the cooling system. From other statements of comparison, automotive radiator is better than cooling tower in terms of installation, size, weight, flexible pipe usage and parasitic load. Therefore, the installation cost and fabrication cost of automotive radiator cooling system will be lower compared to cooling tower. As a conclusion, automotive radiator cooling system is more cost effective compare to cooling tower. Therefore, it is selected as the main cooling device for the introduced cooling system.

CHAPTER 5

CONCLUSION

5.1 Concluding Remarks

As a conclusion, the objective of the theoretical study of automotive radiator and cooling block is to optimize the performance of the automotive radiator cooling system. Theoretical study on the automotive radiator has been carried out to analyze the heat rejection rate in the function of temperature difference between radiator and ambient with different water flow rates and wind speeds (Chong and Tan, 2012). According to the theoretical study of automotive radiator, when the temperature difference between radiator and environment is 15 °C, (which estimate the surface temperature of radiator is 50 °C and the temperature of environment is 35 °C), the chosen automotive radiator (with 3 ms⁻¹ wind speed and 2.2 m² heat dissipate area covered under the fan) is capable to dissipate around 3000 W of solar power input.

Moreover, the performance of specially designed cooling block has been studied separately using different methods: CFD program and analytical formulas (Chong and Tan, 2012). From the theoretical study of cooling block, when solar

heat flux input to the cooling block is 300 kWm^{-2} and water inlet temperature is around $30 \text{ }^\circ\text{C}$, the proposed cooling system with is 0.583 kgs^{-1} water mass flow rate is capable to absorb the excess heat power and transfer to the cooling water to maintain the cooling block's temperature around $50 \text{ }^\circ\text{C}$.

To verify the theoretical modeling on the automotive radiator cooling system, experiments were carried out for on-site data collection using prototype NIPC with total reflective area of 4.16 m^2 and solar concentration of 377 suns. From the result of real-time data collection, the automotive radiator is capable to remove the absorbed heat and maintain the maximum temperature of cooling block well below $50 \text{ }^\circ\text{C}$ (Chong and Tan, 2012). Therefore, the cooling system with specification of 3 ms^{-1} wind speed, 2.2 m^2 heat transfer area and 0.583kgs^{-1} water mass flow is capable to remove the excess heat which is same amount with the solar power input and keep the temperature of cooling block low.

Besides that, the experiment has been conducted to obtain the relationship between the electrical conversion efficiency of CPV module and the cell temperature. From the on-site data collection, the electrical conversion efficiency of CPV module is of a linear relationship to the CPV cell temperature in which the conversion efficiency reduces 0.14% for every 1°C increment in the temperature. For the prototype NIPC, the highest net electrical power output is 665.3 W provided that solar power input is 3118.7 W and conversion efficiency is 26.16 %

with both fan and water pump are switched on (Chong and Tan, 2012).

5.2 Future Work

To further extend the current research work, a thorough study can be conducted on other cooling methods which are more advanced and sophisticated. Since the automotive radiator cooling system is only suitable for small scale NIPC which the reflected solar power to CPV is about 3000 W to 4000 W due to the limitation by fan speed and surface area of radiator which the maximum surface area of radiator is only 2.2 m² and wind speed is only 3 ms⁻¹. According to Figure 4.1, the maximum temperature difference between radiator and environment is about 20 °C (which radiator is 50 °C and environment is 30 °C), the maximum heat rejection rate of radiator is 4000 W.

For bigger size NIPC which the solar power input are more than 4000 W, other cooling device which has higher cooling capacity shall be selected such as cooling tower. According to Table 4.1, cooling tower has higher cooling capacity compare to automotive radiator.

The aim of future study is to determine the best cooling method for CPV with higher cooling capacity and lower parasitic load in order to obtain higher CPV conversion efficiency.

REFERENCES

Aas, G.M.D., and Hansen, L.G.D., 2008. *Photovoltaic Apparatus*. US Patent 2008/0006320 A1. VA: United States of America.

Araki, K., Uozumi, H., Yamaguchi, M., 2002. A simple passive cooling structure and its heat analysis for 500X concentrator PV module. *29th IEEE PVSC* 20 – 24 May 2002 , pp. 1568 – 1571.

Barrau, J., et al., 2011. Effect of a hybrid jet impingement/micro-channel cooling device on the performance of densely packed PV cells under high concentration. *Solar Energy*, 85, pp. 2655 – 2665.

*more than 3 authors

Blundell, S. and Blundell, K., 2006. *Concepts in Modern Physics*. Oxford University Press, pp. 247.

Çengel, A.Y., 2003. *Heat Transfer: a practical approach*, McGraw-Hill series in mechanical engineering, 2nd ed. Boston: McGraw-Hill.

Chong, K.K., et al., 2009. Design and construction of non-imaging planar concentrator for concentrator photovoltaic system. *Renewable Energy*, 34, pp. 1364 – 1370.

*more than 3 authors

Chong, K.K., et al., 2009. Integration of on-axis general sun-tracking formula in the algorithm of open-loop sun-tracking system. *Sensors*, 9, pp. 7849 – 7865.

*more than 3 authors

Chong, K.K., et al., 2010. Optical characterization of nonimaging planar concentrator for the application in concentrator photovoltaic system. *Journal of Solar Engineering*, 132, 011011, pp. 1 – 9.

*more than 3 authors

Chong, K.K. and Tan, W.C., 2012. Study of automotive radiator cooling system for dense-array concentration photovoltaic system. *Solar Energy*, 86(9), pp. 2632-2643.

Chong, K.K. and Wong, C.W., 2011. Application of On-Axis General Sun-Tracking Formula in Open-Loop Sun-Tracking System for Achieving Tracking Accuracy of below 1 mrad. *International Journal of Energy Engineering*, 1(1), pp. 1 – 9.

Cooling Technology Institute, 2012. *Cooling Technology, Education, What is Cooling Tower* [Online]. Available at:

<http://www.cti.org/whatis/coolingtowerdetail.shtml> [Accessed: 20 March 2013]

Cui, M., Chen, N., Yang, X., 2009. Thermal analysis and test for single concentrator solar cells. *Journal of Semiconductors*, 30(4), 044011, pp. 1 – 4.

Dalal, V.L. and Moore, A.R., 1977. Design considerations for high-intensity solar cells, *Journal of Applied Physics.*, 48(3), pp. 1244 – 1251.

Edenburn, M.W., 1980. Active and passive cooling for concentrating photovoltaic arrays. *14th IEEE PVSC*, pp. 776 – 776.

Emcore, 2010. *CJT photovoltaic cell – 10 mm × 10 mm, triple junction solar cell for terrestrial applications, Part no. 615016* [Online]. Available at: <http://www.emcore.com> [Accessed: 4 July 2012]

Fork, D.K. and Horne, S.J., 2007. *Passively Cooled Solar Concentrating Photovoltaic Device*. Palo Alto Research Center Incorporated. US Patent US2007/0256724 A1. Minneapolis: United States of America.

Geankoplis, C.J., 2003. *Transport processes and separation process principles* (includes unit operations), 4th ed. Upper Saddle River, NJ: Prentice Hall Professional Technical Reference.

Horne, W.E., 1993. *Solar energy system*. United Solar Technologies Incorporated. Patent US5269851. United States of America.

Incropera, et al., 2007. *Fundamental of heat and mass transfer*: Wiley Asia student edition, 6th ed. Asia: John Wiley & Sons Pte. Ltd.

*more than 3 authors

Jambunathan, K., et al., 1992. A review of heat transfer data for single circular jet impingement. *International Journal of Heat and Fluid Flow*, 13(2), pp. 106 – 115.

*more than 3 authors

Jinling Refrigeration, 2009. *JLT Jinling Refrigeration catalogue 2009B* [Online]. Available at: <http://www.cnjinling.com> [Accessed: 4 July 2012]

Kreske, K., 2002. Optical design of a solar flux homogenizer for concentrating photovoltaic. *Applied. Optics.*, 41(10), pp. 2053 – 2058.

Lasich, J.B., 2002. *Cooling circuit for receiver of solar radiation*. Patent WO02080286, Australia.

Liu, L., et al., 2011. Heat dissipation performance of silicon solar cells by direct dielectric liquid immersion under intensified illuminations. *Solar Energy*, 85(5), pp. 922 – 930.

*more than 3 authors

Luque, A.L. and Andreev, V.M., 2007. *Photovoltaic concentrator*. New York: Springer Berlin Heidelberg.

Luque, A., et al., 1997. Some results of the EUCLIDES photovoltaic concentrator prototype. *Progress in Photovoltaics: Research and Applications*, 5(3), pp. 195 – 212.

*more than 3 authors

Martin, H., 1977. *Advances in Heat Transfer*. pp. 1 – 60.

Mbewe, D.J., Card, H.C., Card, D.C., 1985. A model of silicon solar cells for concentrator photovoltaic and photovoltaic thermal system design. *Solar Energy*, 35(3), pp. 247 – 258.

Minano, J.C., Gonzalez, J.C., Zanesco, I., 1994. Flat high concentration devices. *24th IEEE PVSC*, Hawaii, pp. 1123 – 1126.

Rodi, W., 1980. Turbulence models for environmental flows. In: W. Knollmann (eds.). *Prediction methods for turbulent flows*. London: Hemisphere Publ. Corp., pp. 259 – 350.

Royne, A., 2005. *Cooling devices for densely packed, high concentration PV arrays*. M.Sc. thesis, School of Physics, University of Sydney, Sydney, Australia.

Royne, A. and Dey, C.J., 2007. Design of a jet impingement cooling device for densely packed PV cells under high concentration. *Solar Energy*, 81, pp. 1014 – 1024.

Royne, A., Dey, C.J., Mills, D.R., 2005. Cooling of photovoltaic cells under concentrated illumination: critical review. *Solar Energy Materials and Solar Cells*, 86, pp. 451 – 483.

Ryu, J.H., Choi, D.H., Kim S.J., 2002. Numerical Optimization of the thermal performance of a microchannel heat sink. *International Journal of Heat and Mass Transfer*, 45(13), pp. 2823 – 2827.

Sala, G., 1989. *Cells and Optics for Photovoltaic Concentration*. Bristol: Adam Hilger, pp. 239 – 267.

Versteeg, H.K. and Malalasekera, W., 1995. *An Introduction to Computational Fluid Dynamics*. London: Longman Group.

Vincenzi, D., et al., 2002. Micromachined silicon heat exchanger for water cooling of concentrator solar cells. *Conference record PV in Europe Conference and Exhibition–From PV technology to Energy Solutions*, 7 – 11 October 2002 Rome, Italy.

*more than 3 authors

Vincenzi, D., et al., 2003. Micromachined silicon heat exchanger for water cooling of concentrator solar cells. *Proceedings of ISES Solar World Congress*, 16 – 19 June 2003 Gothenburg, Sweden.

*more than 3 authors

Webb, B.W. and Ma, C.F., 1995. Single-phase liquid jet impingement heat transfer. In: *Advances in Heat Transfer*. pp. 105 – 217.

Zahedi A., 2010. Review of modeling details in relation to low-concentration solar concentrating photovoltaic. *Renewable and Sustainable Energy Reviews*, 15, pp. 1609 – 1614.

Zhu, L., et al., 2009. An effective heat dissipation method for densely packed solar cells under high concentrations. *Solar Energy Materials & Solar Cells*, 94, pp. 133 – 140.

*more than 3 authors

Zhu, L., et al., 2010. Water immersion cooling of PV cells in a high concentration system. *Solar Energy Materials & Solar Cells*, 95, pp. 538 – 545.

*more than 3 authors

Zukauskas, A., 1972. Heat Transfer from Tubes in Cross Flow. In: Hartnett and T.F. Irvine, Jr., (eds). *Advances in Heat Transfer*, Vol. 8. New York: Academic Press, pp. 93 – 160.



Study of automotive radiator cooling system for dense-array concentration photovoltaic system

Kok-Keong Chong*, Woei-Chong Tan

Faculty of Engineering and Science, Universiti Tunku Abdul Rahman, Off Jalan Gasing Kelang, Setapak, 53300 Kuala Lumpur, Malaysia

Received 16 January 2012; received in revised form 11 May 2012; accepted 31 May 2012

Communicated by: Associate Editor Brian Norton

Abstract

An automotive radiator is proposed for the heat rejection of the dense-array concentrator photovoltaic (CPV) system. Theoretical modeling on the integration of automotive radiator into the cooling system with a specially designed cooling block has been carried out in details. To verify the feasibility of new proposal, the automotive radiator cooling system has been constructed and tested to effectively lower down the temperature of CPV module in a non-imaging planar concentrator prototype with total reflective area of 4.16 m² at solar concentration ratio of 377 suns. During the on-site measurement, it has been observed that the conversion efficiency of CPV module has successfully improved from 22.39% to 26.85% when the CPV cell temperature is reduced from 59.4 °C to 37.1 °C.
© 2012 Elsevier Ltd. All rights reserved.

Keywords: Automotive radiator; Concentrator photovoltaic; High concentration solar energy; Cooling system; Non-imaging planar concentrator; Heat rejection

1. Introduction

High Concentrator Photovoltaic (HCPV) is one of the most effective devices to reduce the cost in solar power generation. In these systems, the HCPV solar cells exposed to very high solar illumination can claim higher conversion efficiency and reduce the expensive solar cell area by replacing it with a cost effective concentrator material. Under highly concentrated sunlight, the solar cell will also inevitably experience a very high heat load that can deteriorate the conversion efficiency if the increasing temperature of the solar cell is not properly managed (Dalal and Moore, 1977; Mbewe et al., 1985; Sala, 1989). According to Cui et al. (2009), a single solar cell can reach extremely high temperature up to 1200 °C with the absence of cooling system at 400 suns, whilst the temperature can be dramatically

reduced by attaching it to a metal panel as cooling panel. Therefore, a reliable heat dissipation system is necessary in HCPV system to continuously cool the solar cells effectively in order to maintain their best performance in all times (Royne et al., 2005). To achieve this goal, there are many cooling techniques have been invented and developed with different cooling performances. Not all cooling techniques are applicable for dense-array HCPV system in which a very rapid cooling is necessary for densely packed CPV cells in a relatively small area.

In the current HCPV system, there are two types of heat rejection systems namely passive and active cooling systems. For passive cooling system, Araki et al. (2002) developed a passive heat dissipation device to dissipate solar cells' heat operating at 500 suns; Fork and Home (2007) patented cooling system that is able to cool the solar cells passively under multi-reflective concentrations with large thermal radiation surface area; Aes and Hansen (2008) patented a cooling apparatus for photovoltaic panels in which the basis layer of the cooling apparatus was designed with

* Corresponding author. Tel.: +60 3 41079802; fax: +60 3 41079803.
E-mail addresses: chongkk@utar.edu.my, kokkeong_o@yahoo.com (K.-K. Chong).

Nomenclature

$A_{connection}$	the total surface area involved in the heat transfer via forced convection (m^2)	R_{solder}	thermal resistance of solder (K/W)
$A_{radiation}$	the total surface area for heat transfer via radiation (m^2)	$R_{sub-copper}$	thermal resistance of substrate copper layer in Direct Bond Copper (K/W)
A_c	cross-sectional area (m^2)	R_{tot}	total thermal resistance (K/W)
A_r	total area of mirrors which reflect the solar flux to the target of NIPC (m^2)	Re_D	Reynolds number of forced convection within radiator and air
c	heat capacity of water ($J\ kg^{-1}\ K^{-1}$)	Re_L	Reynolds number of forced convection within cooling block and water
D_h	hydraulic diameter (m)	T	temperature ($^{\circ}C$)
DNI	direct normal irradiance, $W\ m^{-2}$	T_{amb}	ambient temperature ($^{\circ}C$)
h	heat transfer coefficient ($W\ m^{-2}\ K^{-1}$)	T_{cal}	cooling block's temperature in calculation ($^{\circ}C$)
I_{sc}	short circuit current (A)	T_{CPV}	CPV cell temperature ($^{\circ}C$)
k	turbulent kinetic energy ($m^2\ s^{-2}$)	T_r	average surface temperature of radiator ($^{\circ}C$)
k_a	thermal conductivity of air ($W\ m^{-1}\ K^{-1}$)	T_{sim}	cooling block's temperature in simulation ($^{\circ}C$)
$k_{DBC-alumina}$	thermal conductivity of alumina layer in direct bond copper (DBC) substrate ($W\ m^{-1}\ K^{-1}$)	u_x, u_y	velocity components ($m\ s^{-1}$)
$k_{arctic\ silver}$	thermal conductivity of arctic silver thermal adhesive ($W\ m^{-1}\ K^{-1}$)	μ_l	laminar dynamic viscosity ($Ns\ m^{-2}$)
k_{CPV}	thermal conductivity of CPV cell ($W\ m^{-1}\ K^{-1}$)	μ_t	turbulent dynamic viscosity ($Ns\ m^{-2}$)
k_{copper}	thermal conductivity of copper cooling block ($W\ m^{-1}\ K^{-1}$)	v_a	wind speed ($m\ s^{-1}$)
k_{solder}	thermal conductivity of solder ($W\ m^{-1}\ K^{-1}$)	v_w	water flow speed ($m\ s^{-1}$)
$k_{DBC-copper}$	thermal conductivity of copper layer in direct bond copper (DBC) substrate ($W\ m^{-1}\ K^{-1}$)	V	voltage (V)
k_w	thermal conductivity of water ($W\ m^{-1}\ K^{-1}$)	V_{oc}	open circuit voltage (V)
L	length parallel to the water flow direction in cooling block	x_i, x_j	coordinates (m)
\dot{m}	mass flow rate of water ($kg\ s^{-1}$)		
Nu_a	Nusselt number of forced convection within radiator and air	Greek symbols	
Nu_w	Nusselt number of forced convection within cooling block and water	ΔT	temperature difference ($^{\circ}C$)
P	perimeter (m)	ε_t	turbulent energy dissipation rate ($m^2\ s^{-2}$)
p	pressure ($N\ m^{-2}$)	ε	surface emissivity
P_{in}	solar power input (W)	μ_a	dynamic viscosity of air ($Ns\ m^{-2}$)
$P_{CPV, in}$	solar power input to single cell module (W)	μ_w	dynamic viscosity of water ($Ns\ m^{-2}$)
$P_{CPV, out}$	electricity power output by single cell module (W)	η	the efficiency of direct conversion from solar energy to thermal energy
Pr_a	Prandtl number (based on air temperature)	ρ	fluid density ($kg\ m^{-3}$)
Pr_w	Prandtl number (based on water temperature)	ρ_a	air density ($kg\ m^{-3}$)
Pr_r	Prandtl number (based on radiator surface temperature)	ρ_w	water density ($kg\ m^{-3}$)
$\dot{Q}_{connection}$	convection heat transfer rate (W)	σ	Stefan-Boltzmann constant ($W\ m^{-2}\ K^{-4}$)
\dot{Q}_{out}	heat rejection rate (W)	σ_k, σ_r	turbulent constant
$\dot{Q}_{radiation}$	radiation heat transfer rate (W)	σ_l	laminar Prandtl number
$R_{alumina}$	thermal resistance of substrate alumina in Direct Bond Copper (K/W)	σ_t	turbulent Prandtl number
$R_{arctic\ silver}$	thermal resistance of arctic silver adhesive (K/W)		
R_{CPV}	thermal resistance of CPV cell (K/W)	Subscripts	
R_{copper}	thermal resistance of copper cooling block (K/W)	a	air
		amb	ambient
		c	cross-section
		cal	calculation
		D	diameter
		ε	turbulent energy dissipation rate
		h	hydraulic
		i	i -direction
		j	j -direction
		k	turbulent kinetic energy
		L	parallel length
		l	laminar

<i>r</i>	reflective area	<i>t</i>	turbulent
<i>s</i>	surface	<i>w</i>	water
<i>sim</i>	simulation		

many protruding structure fixed to back side of the panels. Most of the passive cooling systems are only applied to a single solar cell or a linearly array solar cell geometries, but there is no report on any passive cooling system applied to dense array solar cell geometries at very high solar illumination yet.

Densely packed solar cell geometries always encounter high input of heat flux and most of the passive cooling systems with low heat rejection rate would not be good enough to dissipate the heat flux with its limited surface area. Thus, active cooling system with rapid heat dissipation capability provides the only solution for the dense array solar cell geometries. Lasich (2002) patented an active cooling system with water circulation for densely array solar cells under high solar concentrations that is capable to dissipate heat flux 500 kW m^{-2} from the solar cells and to maintain the solar cells' temperature at around $40 \text{ }^\circ\text{C}$. The concept is based on the water flow in many small and parallel channels having good thermal contact with solar cells. Royné and Dey (2007) proposed a cooling device for dense array photovoltaic cells under high solar concentration using jet impingement. An array of jets constitutes the cooling device where the cooling fluid is then drained around the sides in the direction normal to the jet impinging surface. Extensive studies of jet impingement methods were carried out by several research groups, i.e. Martin (1977), Webb and Ma (1995), Jambunathan et al. (1992), Royné (2005). Conversely, Zhu et al. (2009) proposed an efficient liquid-immersion cooling method for dissipating heat from dense array solar cells at high solar concentration level. In their study, the direct-contact heat transfer performance was investigated at different solar concentration level, liquid temperatures and fluid flow velocities.

In this paper, a cost effective and off-the-shelf active cooling device for dense-array concentrator photovoltaic (CPV) system is explored, using an automotive radiator as the main component of heat rejection in the cooling system. Automotive radiator has high heat dissipation profile and does not consume high power like other cooling devices such as industrial cooling tower and chiller. The automotive radiator is easily available, light weight and compact, and hence the proposed setup of cooling system is easy to establish. In this system, water is used as the service fluid and not as complex as dielectric water required by Zhu et al. (2010). The novelty of our study is to integrate an automotive radiator as part of the cooling system in the dense-array CPV system. Theoretical analysis and on-site data collection have been accomplished for the automotive radiator cooling system to verify the feasibility of

our proposal. Furthermore, the conversion efficiency of concentrator photovoltaic module has been measured for different operating temperatures to justify the significance of cooling system in maintaining the good performance of CPV system.

2. Theoretical study

The theoretical modeling of the automotive radiator cooling system had been carried out before the experimental result was acquired in the on-site testing. A three-dimensional (3-D) modeling was established to simulate the temperature at the central point (the hottest point) of the cooling block by varying solar heat flux input, water mass flow rate and water inlet temperature to the cooling block. Moreover, the heat rejection by the automotive radiator was computed by applying the formulas of heat transfer at different wind speeds created by the fan and different surface areas of cooling fins in the radiator. The objective of theoretical modeling for both the automotive radiator and cooling block is to help us in optimizing the designed parameters of the prototype cooling system such as wind speed and water flow rate. The detailed theoretical study and simulation result are presented in the following sections.

2.1. Theoretical study of automotive radiator

In this section, the heat rejection rate of automotive radiator is studied using analytical methods based on the case of forced convection by air and heat dissipation via radiation. The automotive radiator has a total surface area of 3.8 m^2 in which only 2.2 m^2 of the surface area is covered by a fan. In our analysis of heat rejection, convection is considered only on the regions of the radiator covered by the air-flow created by the fan while radiation is considered on the whole surface area of radiator. The heat transfer rate of the automotive radiator through conduction is negligible and can be ignored. Since the forced convection and radiation are the main factors of heat transfer in the automotive radiator, the total heat removed by the automotive radiator is a summation of heat removed by both forced convection and radiation.

The heat transfer rate by forced convection is described as

$$\dot{Q}_{convection} = hA_{convection}\Delta T \quad (1)$$

where $A_{convection}$ is the total surface area involved in the heat transfer via forced convection, ΔT is the temperature difference between heat transfer area and fluid.

The heat transfer coefficient of forced convection occurred between radiator and air is computed as

$$h = \frac{Nu_a k_a}{D_h} \quad (2)$$

where k_a is the thermal conductivity of air which depends on the ambient temperature, Nu_a is Nusselt number in the case of forced convection between the radiator surface and air.

The hydraulic diameter D_h , which is defined as the effective diameter of a non-circular tubes in the first approximation, can be obtained as

$$D_h \equiv \frac{4A_c}{P} \quad (3)$$

where A_c and P are the cross-sectional area, $6.914 \times 10^{-5} \text{ m}^2$, and the perimeter, 0.0723 m , of the radiator tubes respectively. It is the diameter that should be used in calculating the parameters such as Reynolds number, Re_D and Nusselt number, Nu_a .

Since the automotive radiator consists of an array of 33 non-circular tubes arranged in parallel from top to bottom and the wind created by fan is to flow across the parallel tubes, it is treated as a case of cross flow on a non-circular tube. Hence, the Reynolds number can be obtained as

$$Re_D = \frac{\rho_a v_a D_h}{\mu_a} \quad (4)$$

where ρ_a is the air density, v_a is the wind speed and μ_a is the dynamic viscosity of air. The density and dynamic viscosity can vary dependent on the ambient temperature. According to Zukauskas (1972), the Nusselt number of automotive radiator for the case of cross flow on non-circular tubes can be expressed as

$$Nu_a = C Re_D^m Pr_a^n \left(\frac{Pr_a}{Pr_s} \right)^{1/4} \quad (5)$$

$$\left[\begin{array}{l} 0.7 \leq Pr_a \leq 500 \\ 1 \leq Re_D \leq 10^6 \end{array} \right]$$

where all the properties (ρ_a , μ_a , Pr_a , k_a) are evaluated based on the air temperature flowed across the radiator (same as ambient temperature) except Pr_s is evaluated based on radiator's surface temperature and given that $n = 0.37$ for $Pr_a \leq 10$ and $m = 0.5$, $C = 0.51$ for Re_D in the range of 40–1000.

For the heat transfer rate by radiation,

$$\dot{Q}_{radiation} = \varepsilon \sigma A_{radiation} (T_s^4 - T_{amb}^4) \quad (6)$$

where ε is the emissivity of the radiator surface with values ranging from 0 to 1 depending on different surface finishing and material. Incropera et al. (2007) provided a list of emissivity for various materials. Since the automotive radiation is painted in black, therefore the surface emissivity of the whole radiator is stated as 0.98 (Incropera et al., 2007). σ is the Stefan–Boltzmann constant, $5.67 \times 10^{-8} \text{ W m}^{-2} \text{ K}^{-4}$. $A_{radiation}$ is the total surface area for heat transfer via

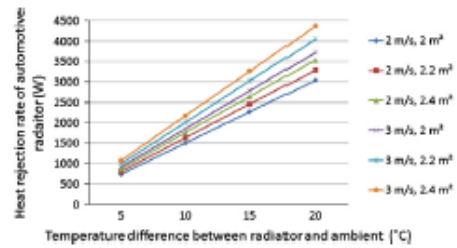


Fig. 1. The graphs of heat rejection rate of automotive radiator versus temperature difference between radiator and ambient for different wind speeds and the heat transfer areas of radiator.

radiation. T_s is the average temperature of radiative surface and T_{amb} is the ambient temperature.

Fig. 1 shows the change of heat rejection rate by automotive radiator in the function of temperature difference between the radiator and ambient for wind speeds at 2 m s^{-1} and 3 m s^{-1} across the radiator provided that the heat transfer surface area are 2.0 m^2 , 2.2 m^2 and 2.4 m^2 . From the chart, the heat rejection rate by the radiator has a linear relationship with the temperature difference between radiator and ambient. A higher temperature difference leading to a higher heat rejection rate fulfills the expression in Eqs. (1) and (6). From Fig. 1, the slope of graph for heat rejection rate versus temperature difference increases with the increase of wind speed and heat transfer area which means that the higher the wind speed and heat transfer area the higher the heat transfer co-efficient will be.

2.2. Simulation of cooling block

A Computational Fluid Dynamic (CFD) program is employed to perform a flow and heat transfer analysis to a specially designed cooling block for the dense array CPV system. In the CFD modeling of the cooling block as illustrated in Fig. 2, its domains comprises of three major parts including cooling block with slot fins, cooling

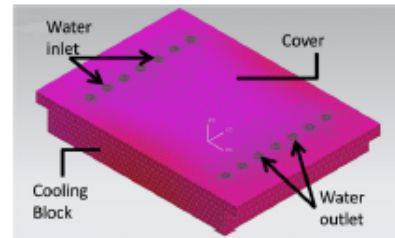


Fig. 2. Drawing to show the CFD modeling for the cooling block where its domains comprises of three major parts including cooling block with slot fins, cooling block cover and water acting as cooling fluid.

Please cite this article in press as: Chong, K.-K., Tan, W.-C. Study of automotive radiator cooling system for dense-array concentration photovoltaic system. Sol. Energy (2012), <http://dx.doi.org/10.1016/j.solener.2012.05.033>

block cover and water acting as cooling fluid. These three parts are meshed using tetrahedral meshing method into a total of 83,835 finite elements with spacing of 5 mm in size wherein 34,785 elements for the cooling block, 21,578 elements for the cover and 27,469 elements for the fluid. All the surfaces in contact between these three parts must be well defined. To start the iteration of simulation, the fluid inside the cooling block is assumed to have incompressible flow at the steady-state. The 3-D governing equations of mass, momentum, energy, turbulent kinetic energy and turbulent kinetic energy dissipation rate in the steady-state are listed as follow (Versteeg and Malalasekera, 1995):

Continuity equation:

$$\frac{\partial \rho \bar{u}_i}{\partial x_i} = 0 \quad (7)$$

Momentum equation:

$$\rho \bar{u}_j \frac{\partial \bar{u}_i}{\partial x_j} = -\frac{\partial \bar{p}}{\partial x_i} + \frac{\partial}{\partial x_j} \left[\mu_t \left(\frac{\partial \bar{u}_i}{\partial x_j} + \frac{\partial \bar{u}_j}{\partial x_i} \right) \right] \quad (8)$$

Energy equation:

$$\rho \bar{u}_j \frac{\partial \bar{T}}{\partial x_j} = \frac{\partial}{\partial x_j} \left[\left(\frac{\mu_t}{\sigma_t} + \frac{\mu}{\sigma_t} \right) \frac{\partial \bar{T}}{\partial x_j} \right] \quad (9)$$

Turbulent kinetic energy (k) equation:

$$\rho \bar{u}_j \frac{\partial k}{\partial x_j} = \frac{\partial}{\partial x_j} \left(\frac{\mu_t}{\sigma_k} \frac{\partial k}{\partial x_j} \right) + \mu_t \left(\frac{\partial \bar{u}_i}{\partial x_j} + \frac{\partial \bar{u}_j}{\partial x_i} \right) \frac{\partial \bar{u}_i}{\partial x_j} - k \varepsilon \quad (10)$$

Turbulent kinetic energy dissipation (ε) equation:

$$\rho \bar{u}_j \frac{\partial \varepsilon}{\partial x_j} = \frac{\partial}{\partial x_j} \left(\frac{\mu_t}{\sigma_\varepsilon} \frac{\partial \varepsilon}{\partial x_j} \right) + C_{1\mu} \mu_t \frac{\varepsilon}{k} \left(\frac{\partial \bar{u}_i}{\partial x_j} + \frac{\partial \bar{u}_j}{\partial x_i} \right) \frac{\partial \bar{u}_i}{\partial x_j} - C_{2\mu} \frac{\varepsilon^2}{k} \quad (11)$$

In the 3-D modeling of cooling block, the k - ε turbulent model is employed which is expressed based on Eqs. (7)–(11). The empirical constants in the above equations are given as: $C_1 = 1.44$, $C_2 = 1.92$, $C_{\mu} = 0.09$, $\sigma_k = 1.0$ and $\sigma_\varepsilon = 1.3$, which are constants for the Standard k - ε model. Full description and calculation for these entire empirical constants were provided by Rodi (1980). With every change of each parameter, 60 computational simulations were executed to obtain the temperature at the center of cooling block that is the same location where the measurement is made in our experiment.

In addition to the CFD simulation, the study on cooling block using the analytical formulas similar to that of study on automotive radiator is also carried out but the forced convection in the cooling block is initiated by water instead of air. Thus, Eq. (1) for the forced convection is also applied in this section too. The calculated results using the analytical method are then compared with the CFD simulated results. The flow characteristic of water in the cooling block is similar to that of a finite plate flow with

a finite length. In this case, the Reynolds number for finite plate flow is expressed as

$$Re_L = \frac{\rho_w v_w L}{\mu_w} \quad (12)$$

where L is the length parallel to the water flow direction in cooling block, ρ_w is the density of water, v_w is the water speed, μ_w is the dynamic viscosity of water.

The Nusselt number in the case of forced convection between cooling block and water is

$$Nu_w = 0.453 Re_L^{1/2} Pr_w^{1/3} \quad (13)$$

where Pr_w is the Prandtl number dependent on the temperature of water.

Heat transfer coefficient for forced convection between cooling block and water is

$$h = \frac{Nu_w k_w}{L} \quad (14)$$

where k_w is thermal conductivity of water.

Fig. 3 shows the change of temperature at the center of cooling block as the function of solar heat flux input for different water inlet temperatures to the cooling block, i.e. 30 °C, 40 °C, 50 °C and different mass flow rates, i.e. 0.4 kg s⁻¹, 0.583 kg s⁻¹. From the graphs, the raise in the water inlet temperature to the cooling block can cause the temperature of cooling block to rise for any particular value of solar heat flux input. It is because water with a higher inlet temperature carries more thermal energy than that of lower inlet temperature and hence reduces the temperature difference between cooling block and water. It has subsequently increased the thermal resistance for the heat dissipation from cooling block to water. From the graphs, the temperature of cooling block can be decreased by increasing the water mass flow rate at any specific solar heat flux input. A higher water mass flow rate can lead to a higher water speed profile, which subsequently increases the heat transfer coefficient of convection between cooling block and water for dissipating more heat.

Fig. 3 also shows a comparison between the simulated and calculated results. From the comparison, the simulated results are always slightly higher in the temperature of cooling block compared to that of the calculated results. The average error between the calculated and simulated results is about 1.86% based on the following equation

$$error = \frac{T_{sim} - T_{cal}}{T_{cal}} \times 100\% \quad (15)$$

where T_{sim} is the temperature of cooling block obtained from the CFD simulated result and T_{cal} is the temperature of cooling block obtained from the calculated result.

3. Experimental setup

The experimental setup consists of two major parts, which are non-imaging planar concentrator (NIPC) and automotive radiator cooling system.

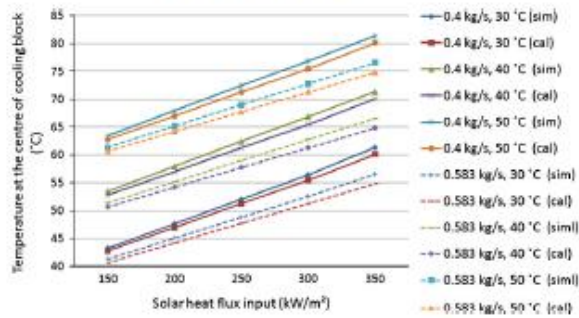


Fig. 3. The graphs of temperature at the center of cooling block versus solar heat flux input for different water inlet temperatures and mass flow rates. (Solid line represents mass flow rate of 0.4 kg s^{-1} and dot line represents mass flow rate of 0.583 kg s^{-1} .)



Fig. 4. Picture to show the prototype of nonimaging planar concentrator that is located at latitude of 3.2°N and longitude of 107.7°E , in the campus of Universiti Tunku Abdul Rahman (UTAR), Kuala Lumpur, Malaysia.

3.1. Non-imaging planar concentrator (NIPC)

A prototype of NIPC has been designed and constructed to serve the purpose of performing sun-tracking and focusing sunlight onto a copper cooling block at focal distance of 1.7 m (Chong et al., 2009a, 2010). The prototype capable of producing a good uniformity of solar illumination consists of 416 flat mirrors with $10 \text{ cm} \times 10 \text{ cm}$ each to form a total reflective area of 4.16 m^2 . Fig. 4 shows a picture of the NIPC prototype located at latitude 3.2°N and longitude 107.7°E , in the campus of Universiti Tunku Abdul Rahman (UTAR), Kuala Lumpur, Malaysia. The azimuth-elevation sun-tracking method has been adapted to the NIPC prototype and each of the axes is driven by a stepper motor

connected to worm gearbox reducer with gear ratio of 60. The mirror frames and the receiver holder frame are made of Aluminum 6061 due to its light weight and low acting torque required for driving the concentrator. A Windows-based program implemented using Microsoft Visual Basic.net was developed to control the sun-tracking mechanism according to the day number of the year, the local time, time zone, latitude and longitude of the prototype installation. The program acquires the aforementioned information for calculating the azimuth and elevation angles of the sun so that the stepper motors will be triggered to drive the concentrator frame to the required orientation (Chong and Wong, 2009b,c, 2011). As the apparent position of the sun changes with time throughout the day, the computer continuously send signals via the parallel

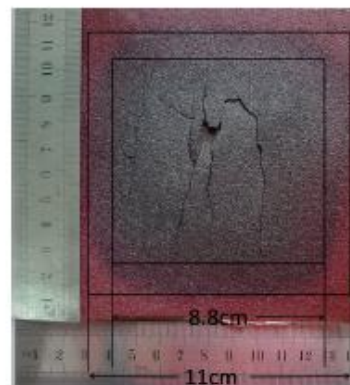


Fig. 5. The concentrated sunlight has generated different grades of burnt mark on the sand paper, where the total area of burnt mark on the sand paper was measured as $11 \text{ cm} \times 11 \text{ cm}$ and a darker carbonized burnt area was measured as $8.8 \text{ cm} \times 8.8 \text{ cm}$.

Please cite this article in press as: Chong, K.-K., Tan, W.-C. Study of automotive radiator cooling system for dense-array concentration photovoltaic system. Sol. Energy (2012), <http://dx.doi.org/10.1016/j.solener.2012.05.033>

port to the driver to adjust the orientation of concentrator frame appropriately about the azimuth and elevation axes for maintaining the tracking position. The tracker is commanded to follow the sun at all times because the program is run in repeated loops to ensure a smooth and continuous movement of the concentrator frame.

The solar flux distribution at the cooling block was investigated by exposing a sand paper to the concentrated sunlight for a few seconds. The concentrated sunlight had generated different degrees of burnt marks on the sand paper as shown in Fig. 5. The total area of the burnt mark on the sand paper was measured as $11\text{ cm} \times 11\text{ cm}$ and a darker burnt area was measured as $8.8\text{ cm} \times 8.8\text{ cm}$. On the other hand, the solar flux distribution profile has been simulated based on the specification of NIPC prototype using ray-tracing method (Chong et al., 2010). Fig. 6a and b displays the simulated result in 3-D and 2-D plots

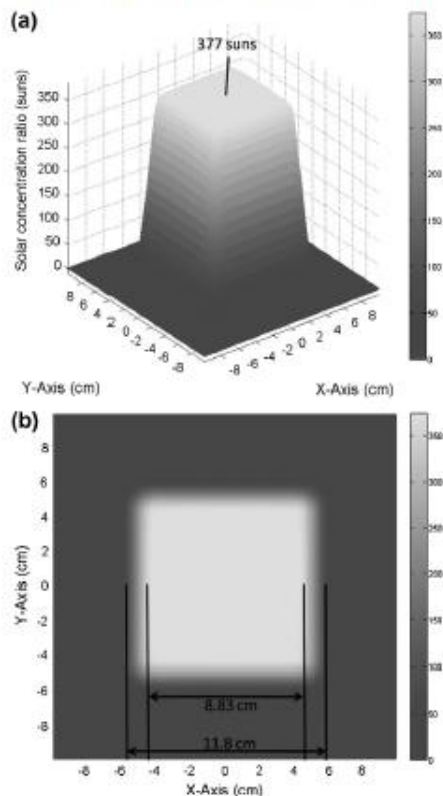


Fig. 6. The simulated results of solar flux distribution for the nonimaging planar concentrator prototype that consists of 420 flat mirrors in (a) 3-D and (b) 2-D plots with a focal distance of 170 cm.

accordingly in which the solar flux profile consists of a flat top area in the central region with maximum solar concentration ratio of 377 suns named as uniform illumination area. The dimension of simulated result is reasonably close to the actual measurement, which is $11.8\text{ cm} \times 11.8\text{ cm}$ in total area and $8.83\text{ cm} \times 8.83\text{ cm}$ in the uniform illumination area.

3.2. Automotive radiator cooling system

The automotive radiator cooling system can be divided into four components, which are automotive radiator, cooling block, water pump, and reservoir tank. Fig. 7 depicts the automotive radiator taken from a “Proton Wira 1500 c.c.” automobile. This automotive radiator has a capacity of 1.5-liter that is used as a key device for the heat rejection in the cooling system. The materials of both the automotive radiator casing and tubes are aluminum alloy with high heat conductivity and light weight. It is easy to be installed to the NIPC prototype with minimum load added to the driving system. The external fins sandwiched between the ducts in the radiator are made of copper in order to have higher heat conductivity for increased heat dissipation rate. The total heat transfer area of the radiator is reasonably large, which includes the surface areas of radiator ducts and of copper fins. From our measurement, the total surface area of radiator ducts is 0.8 m^2 and the total surface area of copper fins is 3 m^2 to result in 3.8 m^2 for the total surface area of the radiator. A 280 mm diameter DC fan with rated power of 50.6 W is attached to the automotive radiator which can create a significant air flow with wind speeds up to 3 m s^{-1} . The Reynolds number for air flow across the radiator Re_D , Nusselt number Nu_D and heat transfer coefficient h are obtained as 730, 12 and $80\text{ W m}^{-2}\text{ K}^{-1}$ respectively.

The cooling block for mounting the dense-array CPV panel is the major component for absorbing and transferring the extra heat rejected by the dense-array CPV panel



Fig. 7. Picture to show the automotive radiator from a commercial automobile with model “Proton Wira 1500 c.c.” with the capacity of 1.5-liter used as the key device for the heat rejection in the cooling system.

Please cite this article in press as: Chong, K.-K., Tan, W.-C.: Study of automotive radiator cooling system for dense-array concentration photovoltaic system. Sol. Energy (2012), <http://dx.doi.org/10.1016/j.solener.2012.05.033>

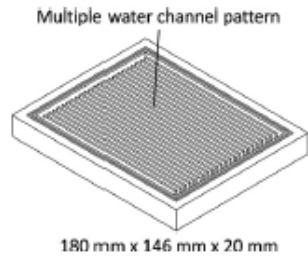


Fig. 8. Drawing to show the cooling block made of a copper with a dimension 180 mm \times 146 mm \times 20 mm machined into a pattern of multiple water channels.

to the cooling water. In this context, the preferred material of the cooling block is copper for its high thermal conductivity. To ensure a high heat transfer rate, the cooling block must also have sufficient surface area and therefore a copper block measuring 180 mm \times 146 mm \times 20 mm was machined with a cavity containing multiple water channels as illustrated in Fig. 8. The multiple water channels have contributed to a large surface area of 1192.20 cm² for the heat transfer between cooling block and water. Besides, this pattern also allow water to pass through it with high speed by making use of the straight and narrow guides that increase the heat transfer coefficient. This cooling block is then covered and shielded with an aluminum plate with a dimension of 204 mm \times 146 mm \times 10 mm.

In the experimental setup, a "Tsunami Pump Nemo-100A" AC submersible water pump with a rated power of 100 W has been utilized for circulating water between the radiator and the cooling block. Its role is to create a constant water speed within the automotive radiator cooling system at mass flow rate of 0.583 kg s⁻¹. The Reynolds number for water flow in the cooling block Re_L , Nusselt number Nu_w and heat transfer coefficient h are obtained as 31,270, 192 and 1967 W m⁻² K⁻¹ respectively.

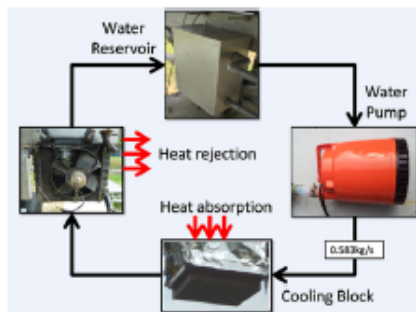


Fig. 9. The schematic diagram to show all the components of the automotive radiator cooling system and the flow direction of water in the experimental setup.

The last component is a reservoir tank which acts as the start point and end point of the water circulation, and storage tank for the submersible water pump in the automotive radiator cooling system.

Fig. 9 is the schematic diagram of the automotive radiator cooling system to illustrate the flow direction of water in the experimental setup. After the water pump is switched on, the water from reservoir tank will be directed to the copper cooling block located at the target of the solar concentrator with a distance of 2.2 m relative to the reservoir. When the water passes through the cooling block, it will absorb the thermal energy from the concentrated sunlight. The temperature of water will rise after the heat absorption and the water will then be headed to the automotive radiator. Inside the automotive radiator, the water is forced to flow through the parallel aluminum ducts evenly in such a way that heat rejection can effectively take part during the process. In the radiator, the thermal energy carried by the water will be rejected to surrounding via forced convection created by the fan. The temperature of water will be lower down in the process of the heat rejection and then be channeled back to the reservoir tank so that a new circulation can be started again. Table 1 summarizes the specification of the whole experimental setup.

4. Result and discussion

To verify the theoretical modeling of the automotive radiator cooling system, real-time data collection was conducted at the site and the measured results were compared with the results attained from the theoretical study. The experiments for collecting data were carried out in two sessions on two different days. During the progression of this process, all the measured parameters were closely monitored and recorded, such as direct normal irradiance (DNI) ranging from 300 W m⁻² to 950 W m⁻², an ambient temperature ranging from 30 °C to 36 °C, and air relative humidity ranging from 45% to 72%. Other parameters in the setting were ascertained to be the same in both experiments, i.e. wind speed of the fan, 3 m s⁻¹, and mass flow rate of water, 0.583 kg s⁻¹. First experiment was only conducted for 20 min wherein the data was collected for every minute. Second experiment was conducted for 6 h from 10.30 a.m. to 4.30 p.m. where each output from the setup is taken at an interval of 15 min apart. The collected data were then used to calculate the solar power input into the automotive radiator cooling system and heat rejection rate of the radiator. The DNI was measured by pyrheliometer and the solar power input can be calculated using the following formula:

$$P_{in} = \eta \times DNI \times A_r \quad (16)$$

where η (≈ 0.8) is the efficiency of direct conversion from solar energy to thermal energy considering the reflection loss of mirror and absorptivity of cooling block, A_r is the total reflective area of the NIPC prototype. The ambient temperature and humidity were measured using an air

Table 1
The specification of experimental setup.

Radiator	
Radiator capacity	1.5-liter
Total surface area	3.8 m ²
Heat transfer area covered by fin	2.2 m ²
Cross section area of radiator ducts, A_c	6.914 × 10 ⁻⁵ m ²
Perimeter of radiator ducts, P	0.0773 m
Air flow boundary diameter (Fan's diameter)	280 mm
Wind speed created by fan, v_a	3 m s ⁻¹
Reynolds number of air across radiator, Re_D	730
Nusselt number of air, Nu_a	12
Heat transfer coefficient of air, h	80 W m ⁻² K ⁻¹
Range of temperature for radiator surface, T_r	From 30 °C to 50 °C
Conductivity of radiator fin	387 W m ⁻¹ K ⁻¹
Conductivity of radiator ducts	170 W m ⁻¹ K ⁻¹
Rated power of fan	50.6 W
Cooling block	
Dimension	180 mm × 146 mm × 20 mm
Number of slot-fins	23
Total surface area of each slot-fin	44.08 cm ²
Total heat transfer surface area	1192.20 cm ²
Conductivity	387 W m ⁻¹ K ⁻¹
Water mass flow rate	0.583 kg s ⁻¹
Reynolds number of water, Re_L	31,270
Nusselt number of water, Nu_w	192
Heat transfer coefficient of water, h	1967 W m ⁻² K ⁻¹
Non-imaging planar concentrator	
Total reflective area, A_r	4.16 m ²
Focal distance	1.70 m
Latitude	3.2°N
Longitude	107.7°E
Rated power of water pump	100 W

quality meter and the heat rejection rate of radiator can be computed from the following formula:

$$\dot{Q}_{out} = \dot{m} \times c \times \Delta T \quad (17)$$

where ΔT is the water temperature difference between inlet and outlet of radiator; \dot{m} is mass flow rate of water (0.583 kg s⁻¹) and c is heat capacity of water (4200 J kg⁻¹ K⁻¹).

In Fig. 10, solar power input, heat rejection rate and the temperature at the center of cooling block are plotted versus time (minutes) for the first experiment. From the graphs, the solar power input is reasonably constant throughout the experiment ranging from 2300 W to 2700 W, whilst the heat rejection rate of the radiator increases gradually over time until it reaches about 2400 W. The heat rejection rate saturates in between 2400 W and 2700 W after 14 min of operation. Alternatively, the temperature at the center of cooling block increases gradually in the beginning and then saturates at about 50 °C after 14 min. From the observation, the automotive radiator is capable of removing the equal amount of heat as that of being absorbed by the cooling block and hence reaching thermal equilibrium in the same period of time. In principle, it is plausible that the radiator has the capacity to remove heat at the rate of 2640 W or higher, which is sufficient to equalize the solar power input if the temperature difference between radiator and ambient has achieved 15 °C or higher (or the water temperature of cooling system of 50 °C and the ambient temperature of 30–35 °C) given that $h = 80 \text{ W m}^{-2} \text{ K}^{-1}$ and $A = 2.2 \text{ m}^2$.

Fig. 11 shows the recorded results of the second experiment for a period of 6 h at an interval of 15 min. Referring to Fig. 11, the changes of the graphs can be viewed in four different periods of time, which are 1030–1200 h, 1200–1345 h, 1345–1515 h, and 1515–1630 h. From 1030 h to 1200 h, the solar power input increased from 2133 W to 2708 W in the first 15 min and then maintained within the range from 2544 W to 2749 W. In this period of time, the heat rejection rate during the first half an hour from 1469 W to 2693 W to equalize the solar input power and after that it maintained at the rate of 2693 W until 1200 h. The temperature at the center of cooling block maintained in the range from 47 °C to 51 °C throughout this period which is quite stable. From 1200 h to 1345 h, the solar power input fluctuated drastically within the range from 1025 W to 3118 W caused by the intermittent sunlight. Consequently, the heat rejection rate and temperature at the center of cooling block also followed to fluctuate accordingly in the range of 1469–2693 W and 35–49 °C

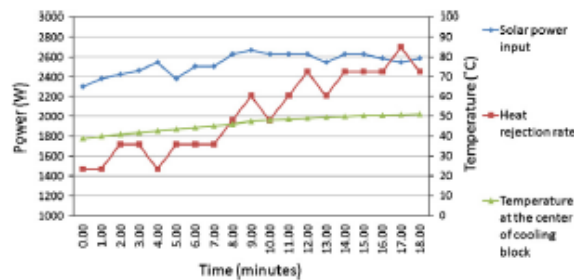


Fig. 10. The graphs of solar power input, heat rejection rate and the temperature at the center of cooling block versus time (minutes) in the first experiment.

Please cite this article in press as: Chong, K.-K., Tan, W.-C. Study of automotive radiator cooling system for dense-array concentration photovoltaic system. Sol. Energy (2012), <http://dx.doi.org/10.1016/j.solener.2012.05.033>

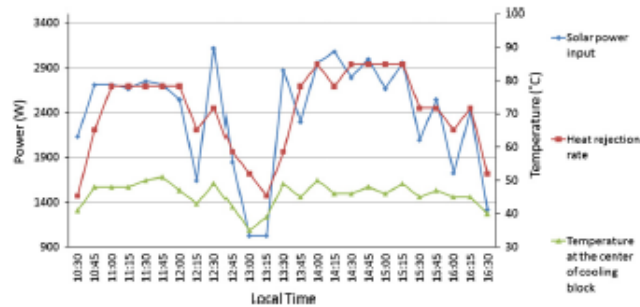


Fig. 11. The graphs of solar power input, heat rejection rate and the temperature at the center of cooling block versus local time for a period of 6 h at the interval of 15 min in the second experiment.

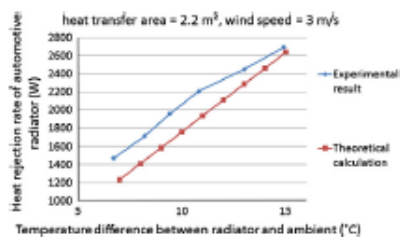


Fig. 12. The graphs to show a comparison for the heat rejection rate of radiator between experimental and theoretical results.

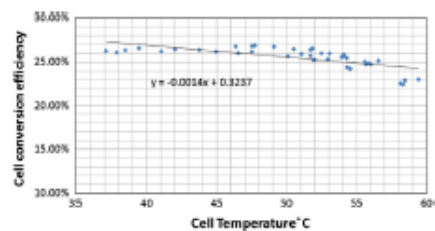


Fig. 14. Graph to show the measured result of electrical conversion efficiency of CPV module versus CPV cell temperature.

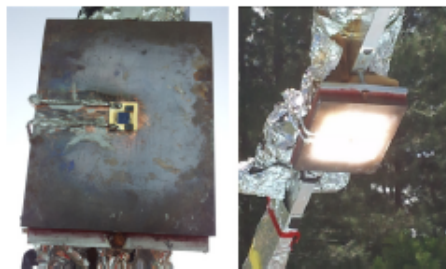


Fig. 13. The left photo shows how the CPV module is attached to cooling block for on-site data collection and the right photo shows the CPV module exposed under high solar concentration during on-site measurement.

respectively. From 1345 h to 1515 h, the solar power input was returned back to a stable condition again, which was in the range from 2298 W to 3077 W. For this period of time, the heat rejection rate and the temperature of cooling block were maintained stably in the range of 2693–2938 W and 45–50 °C respectively. From 1515 h to 1630 h, the solar power input again had dramatic fluctuation within the

range from 1313 W to 2954 W in a decreasing trend. The resulted heat rejection rate and temperature of cooling block were then decreased ranging from 2938 W to 1714 W and from 49 °C to 40 °C respectively to follow the decreasing trend of solar power input. From the observation, the automotive radiator is capable to remove the absorbed heat and to maintain the maximum temperature of cooling block well below 50 °C even though the experiment was continued for 6 h.

Comparing the heat rejection of radiator between experimental and theoretical results as shown in Fig. 12, the heat rejection rate of experimental result is slightly higher than that of theoretical result because there are other sources for the heat lost including conduction, natural convection and radiation. The heat rejection rate for the theoretical result is 91% of the experimental result.

Apart from the study in the heat rejection of automotive radiator, it is also important to understand its effect to the electrical conversion efficiency of the CPV module. As a result, a commercially available single CPV cell receiver module (Emcore, 2010) has been attached to the cooling block of the NIPC prototype. In Fig. 13, the left photo shows how the CPV module is attached to cooling block for on-site data collection and the right photo shows the CPV module exposed under high solar concentration during on-site measurement.

The electrical conversion efficiency of CPV module can be calculated using the formulas stated as follow:

$$\eta_{CPV} = (P_{CPV,out}/P_{CPV,in}) \times 100\% \quad (18)$$

where $P_{CPV,in}$ is the solar power input received by the CPV module and $P_{CPV,out}$ is the electrical power output generated by CPV module

$$P_{CPV,in} = \eta \times \text{DNI} \times A_r \times (A_{CPV}/A_{image}) \quad (19)$$

$$P_{CPV,out} = V_{oc} \times I_{sc} \times 0.87 \quad (20)$$

where A_{CPV} is the total active area of CPV cell ($1 \times 10^{-4} \text{ m}^2$), A_{image} is the total image area of the concentrated sunlight on the cooling block (0.01 m^2), V_{oc} is the measured open circuit voltage of CPV module and I_{sc} is the measured short circuit current of CPV module and 0.87 is the Fill Factor of CPV module provided by Emcore data sheet (2010).

To calculate the temperature of CPV cell, the following formula is used:

$$T_{CPV} = P_{CPV,in} \times R_{tot} \times (1/A_{CPV}) \times (1 - \eta_{CPV}) + T_{CB} \quad (21)$$

where T_{CB} is the temperature of cooling block, R_{tot} is the total thermal resistance from cooling block to CPV cell consisted of the following materials: copper (cooling block), arctic silver thermal adhesive, copper layer in direct bond copper (DBC) substrate, alumina layer in DBC substrate, copper layer in DBC substrate, solder material and CPV cell that can be calculated as:

$$R_{tot} = R_{CPV} + R_{solder} + R_{DBC-copper} + R_{DBC-alumina} + R_{DBC-copper} + R_{arctic silver} + R_{copper} \quad (22)$$

where

$$R_{CPV} = l_{CPV}/k_{CPV}$$

$$R_{solder} = l_{solder}/k_{solder}$$

$$R_{DBC-copper} = l_{DBC-copper}/k_{DBC-copper}$$

$$R_{DBC-alumina} = l_{DBC-alumina}/k_{DBC-alumina}$$

$$R_{arctic silver} = l_{arctic silver}/k_{arctic silver}$$

$$R_{copper} = l_{copper}/k_{copper}$$

where l_{CPV} , l_{solder} , $l_{DBC-copper}$, $l_{DBC-alumina}$, $l_{arctic silver}$, and l_{copper} were the thicknesses of different materials measured as 0.12 mm, 0.15 mm, 0.3 mm, 0.635 mm, 0.1 mm and 5 mm respectively; k_{CPV} , k_{solder} , $k_{DBC-copper}$, $k_{DBC-alumina}$, $k_{arctic silver}$, and k_{copper} are referred as the thermal conductivity of different materials with the values $55 \text{ W m}^{-1} \text{ K}^{-1}$, $29 \text{ W m}^{-1} \text{ K}^{-1}$, $400 \text{ W m}^{-1} \text{ K}^{-1}$, $24 \text{ W m}^{-1} \text{ K}^{-1}$, $7.5 \text{ W m}^{-1} \text{ K}^{-1}$, $400 \text{ W m}^{-1} \text{ K}^{-1}$ respectively, which are provided by Luque and Andreev (2007).

Fig. 14 shows the measured result of electrical conversion efficiency of CPV module versus CPV cell temperatures. The conversion efficiency is of a linear relationship to the cell temperature where the slope of the graph is -0.0014 which means the conversion efficiency reduced by 0.14% for every increment of 1°C . Referring to the graph, the maximum conversion efficiency is 26.85% at

the temperature 47.7°C , whereas the lowest conversion efficiency is 22.39% at the temperature 58.3°C .

There are two possible cases: (1) both water pump and fan are switched on in which the CPV cell temperature is 47.5°C and the resultant conversion efficiency is 26.16%; (2) water pump is switched on but the fan is off in which the CPV cell temperature is raised to 58.08°C while the resultant conversion efficiency is reduced to 22.51%. For the case (1), the electrical output power produced by CPV at conversion efficiency of 26.16% is 66.5 W provided that the DNI is 800 W m^{-2} and the resulted solar power input is 2662.4 W. The net electrical power output will be 545.9 W after subtracting by 150.6 W consumed by both the fan and water pump. For the case (2), the electrical output power produced by CPV at conversion efficiency of 22.51% is 599.3 W provided that the DNI is 800 W m^{-2} and the resulted solar power input is 2662.4 W. The net electrical power output will be 499.3 W after subtracting by 100 W consumed by the water pump only. Comparing the two cases, the first case with the fan on can produce 46.6 W more net power output than the second case without the fan. Hence, we can conclude that efficient cooling system is very significant for CPV system to produce more net electrical power output. From Fig. 11, the highest solar power input is 3118.7 W and therefore the net electrical power output can be as high as 665.3 W provided that the conversion efficiency is 26.16%.

5. Conclusion

Theoretical study on the automotive radiator has been carried out to analyze the heat rejection rate in the function of temperature difference between radiator and ambient for different water flow rates and wind speeds created by fan. Moreover, the performance of specially designed cooling block has been studied separately using different methods: CFD program and analytical formulas. To verify the theoretical modeling on the automotive radiator cooling system, experiments were carried out for on-site data collection using NIPC prototype with total reflective area of 4.16 m^2 and solar concentration of 377 suns. The heat rejection rate obtained in the theoretical result is as high as 91% of the experimental result. Finally, the experiment was also conducted to obtain the relationship between the electrical conversion efficiency of CPV module and the cell temperature. From the on-site data collection, the electrical conversion efficiency of CPV module is of a linear relationship to the CPV cell temperature in which the conversion efficiency reduces 0.14% for every 1°C increment in the cell temperature. For the NIPC prototype, the highest net electrical power output is 665.3 W provided that solar power input is 3118.7 W and conversion efficiency is 26.16%.

Acknowledgements

The authors would like to express their gratitude to Fundamental Research Grant Scheme (FRGS) by the

Ministry of Higher Education with Project number FRGS/1/11/TK/UTAR/03/4 and AAIIBE Trust Fund by Ministry of Energy, Green Technology & Water.

References

- Aes, Lars G., Hansen, Dysterud, 2008. Photovoltaic Apparatus. US Patent 2008/0006320 A1, January 10, 2008, (Gaute Dominic Magnusson).
- Araki, K., Uozumi, H., Yamaguchi, M., 2002. A simple passive cooling structure and its heat analysis for 500X concentrator PV module. In: 29th IEEE PVSC, pp. 1568–1571.
- Chong, K.K., Wong C.W., 2009b. General formula for on-axis sun tracking system and its application in improving tracking accuracy of solar collector. *Solar Energy* 83 (3), 298–305.
- Chong, K.K., Wong, C.W., 2011. Application of on-axis general sun-tracking formula in open-loop sun-tracking system for achieving tracking accuracy of below 1mrad. *International Journal of Energy Engineering* 1 (1), 25–32.
- Chong, K.K., Siaw, F.L., Wong, C.W., Wong, G.S., 2009a. Design and construction of non-imaging planar concentrator for concentrator photovoltaic system. *Renewable Energy* 34 (9), 1364–1370.
- Chong, K.K., Wong, C.W., Siaw, F.L., Yew, T.K., Ng, S.S., Liang, M.S., Lim, Y.S., Lau, S.L., 2009c. Integration of an on-axis general sun-tracking formula in the algorithm of an open-loop sun-tracking system. *Sensors* 9 (10), 7849–7865.
- Chong, K.K., Wong, C.W., Siaw, F.L., Yew, T.K., 2010. Optical characterization of nonimaging planar concentrator for the application in concentrator photovoltaic system. *Journal of Solar Energy Engineering* 132 (1), 011011(1–9).
- Cui, M., Chen, N., Yang, X., et al., 2009. Thermal analysis and test for single concentrator solar cells. *Journal of Semiconductors* 30 (4), 044011(1–4).
- Dalal, V.L., Moore, A.R., 1977. Design considerations for high-intensity solar cells. *Journal of Applied Physics* 48 (3), 1244–1251.
- Emcore, 2010. CJT Photovoltaic Cell – 10 mm × 10 mm, Triple Junction Solar Cell for Terrestrial Applications, Part No. 615016. Data sheet. Retrieved from <<http://www.emcore.com>>.
- Fork, David K., Horne, Stephen J., 2007. Passively Cooled Solar Concentrating Photovoltaic Device. US Patent US2007/0256724 A1, November 8, 2007.
- Incropera, F.P., Dewitt, D.P., Bergman, T.L., Lavine, A.S., 2007. *Fundamental of Heat and Mass Transfer*, sixth ed. John Wiley & Sons, Printed in Asia, pp. 9–13 (ISBN-13: 978-0-471-79471-4).
- Jambunathan, K., Lai, E., Moss, M.A., Button, B.L., 1992. A review of heat transfer data for single circular jet impingement. *International Journal of Heat and Fluid Flow* 13 (2), 106–115.
- Lasich, J.B., 2002. Cooling Circuit for Receiver of Solar Radiation. Patent WO02080286, Australia.
- Luque, A.L., Andreev, V.M., 2007. *Photovoltaic Concentrator*. Springer, Berlin Heidelberg New York (ISBN-13: 978-3-540-68796-2).
- Martin, H., 1977. Heat and mass transfer between impinging gas jets and solid surfaces. *Advances in Heat Transfer* Chp 13, 1–60.
- Mbewe, D.J., Card, H.C., Card, D.C., 1985. A model of silicon solar cells for concentrator photovoltaic and photovoltaic thermal system design. *Solar Energy* 35 (3), 247–258.
- Rodi, W., 1980. Turbulence models for environmental flows. In: Knollmann, W. (Ed.), *Prediction Methods for Turbulent Flows*. Hemisphere Publ. Corp., London, pp. 259–330.
- Royne, A., 2005. *Cooling Devices for Densely Packed, High Concentration PV Arrays*. MSc thesis, School of Physics, University of Sydney, Sydney, Australia.
- Royne, A., Dey, C.J., 2007. Design of a jet impingement cooling device for densely packed PV cells under high concentration. *Solar Energy* 81, 1014–1024.
- Royne, A., Dey, C.J., Mills, D.R., 2005. Cooling of photovoltaic cells under concentrated illumination: critical review. *Solar Energy Materials and Solar Cells* 86, 451–483.
- Sala, G., 1989. Chp 8: Cooling of solar cells, in: *Cells and Optics for Photovoltaic Concentration*. Adam Hilger, Bristol, pp. 239–267.
- Versteeg, H.K., Malalasekera, W., 1995. *Computational Fluid Dynamics*. Longman Group.
- Webb, B.W., Ma, C.-F., 1995. Single-phase liquid jet impingement heat transfer. *Advances in Heat Transfer* Chp 26, 105–217.
- Zhu, L., Wang, Y., Fang, Z., Sun, Y., Huang, Q., 2009. An effective heat dissipation method for densely packed solar cells under high concentration. *Solar Energy Materials and Solar Cells* 94, 133–140.
- Zhu, L., Boehm, R.F., Wang, Y., Halford, C., Sun, Y., 2010. Water immersion cooling of PV cells in a high concentration system. *Solar Energy Materials and Solar Cells* 95, 538–545.
- Zukauskas, A., 1972. Heat transfer from tubes in cross flow. In: Hartnett, Irvine, T.F., Jr. (Eds.), *Advances in Heat Transfer*, vol. 8. Academic Press, New York.



Tsunami Pump™

your preferred water booster

SEWAGE SUBMERSIBLE PUMP



Low Maintenance



Energy Saving



304 Anti-Rust
Pump Shell



316L Anti-Corrosive
Stainless Steel
Motor Shaft



1 Year
Warranty



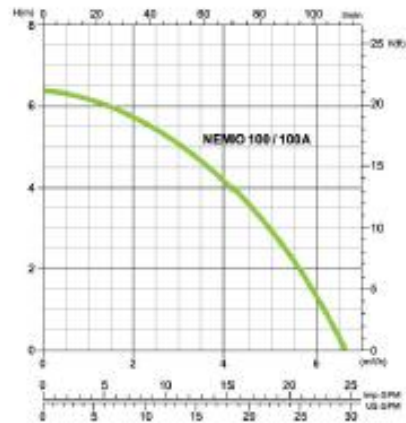
Over Heating
Protection

日本の新しい技術 Tokyo (JP) New Technology



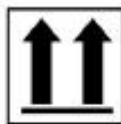
SEWAGE SUBMERSIBLE PUMP

- Italian dual mechanical seal
- Imported thermal protection device
- 316L Stainless Steel Shaft
- Pump shell can be AISI304 or Plastic
- Suitable for fish pond and household uses



Performance Table

Model	Power		Voltage V	Max Flow m³/h	Max Head m	Outlet mm
	W	HP				
NEMO 100	100	1/8	220/230/240	6.5	6.3	11/18.5
NEMO 100A	100	1/8	220/230/240	6.5	6.3	11/18.5



APPENDIX C

Hurricane Pumps

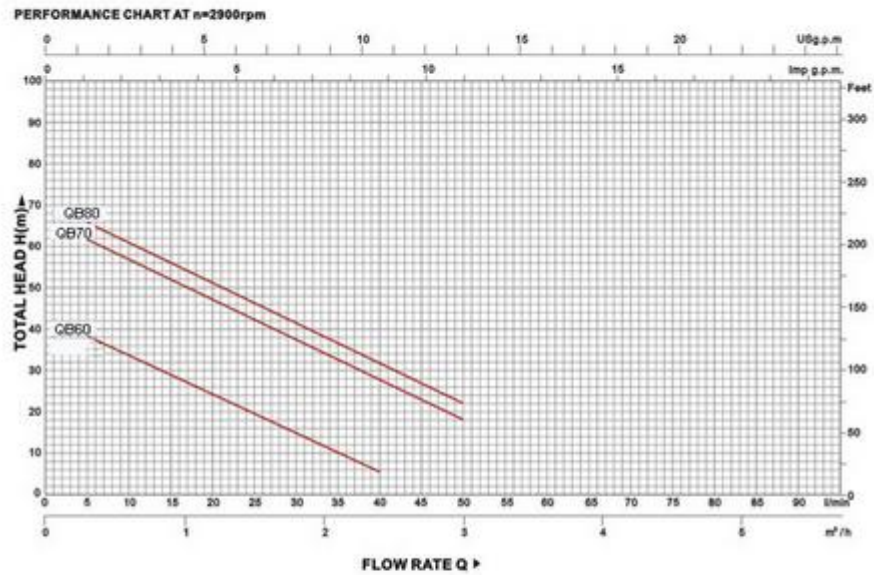
QB60 Booster Pump 220V 370W

[<<click here>>](#) or on the picture below for an instant, printable online quotation.



Structure

- ◆ Cast Iron pump Body
- ◆ SS Mechanical Seal (Graphite to Ceramic)
- ◆ Steel or Stainless Steel Shaft
- ◆ Brass impeller with radial peripheral blades
- ◆ Aluminium or copper wire
- ◆ Thermal Protector



Technical Data Hurricane Pumps Submersable Pump 220V 370W	
Description	Data
Model	QB60
Pump	Booster Pump
Voltage	220V
Power	370W
Head Height	35m
Maximum Output	2100L/Hour
Size	1" x 1"



Hurricane Pumps
Tel : 015 297 2444
Phillip Venter : 083 450 3321
Email : info@hurricanepumps.co.za